THEORY OF A HELICAL RESONATOR PLASMA SOURCE

by

M. A. Lieberman, A. J. Lichtenberg, and D. L. Flamm

Memorandum No. UCB/ERL M90/10

5 February 1990

THEORY OF A HELICAL RESONATOR PLASMA SOURCE

by

M. A. Lieberman, A. J. Lichtenberg, and D. L. Flamm

Memorandum No. UCB/ERL M90/10

5 February 1990

ELECTRONICS RESEARCH LABORATORY

College of Engineering
University of California, Berkeley
94720

THEORY OF A HELICAL RESONATOR PLASMA SOURCE

by

M. A. Lieberman, A. J. Lichtenberg, and D. L. Flamm

Memorandum No. UCB/ERL M90/10

5 February 1990

ELECTRONICS RESEARCH LABORATORY

College of Engineering
University of California, Berkeley
94720

Theory of a Helical Resonator Plasma Source

by

M.A. Lieberman, A.J. Lichtenberg and D.L. Flamm

Department of Electrical Engineering and Computer Sciences

and the Electronics Research Laboratory

University of California, Berkeley, CA 94720

ABSTRACT

A helical resonator plasma source is a resonant, slow wave, plasma-loaded structure consisting of a cylindrical plasma surrounded by a helical coil which, in turn, is surrounded by a grounded coaxial cylinder. Such sources can be efficiently matched to an external power source and can operate at low gas pressures. We employ a developed sheath helix model, in which the cylindrical geometry is unfolded into a rectangular geometry and the RF current in the helix wires is replaced by a continuous current sheet, to obtain the dispersion characteristics (β versus ω, where β is the axial wavenumber and ω is the frequency) for the slow waves, their electric and magnetic fields, and the scaling of the dispersion and fields with source parameters and geometry. We use a quasistatic approximation to obtain the fields in a cylindrical structure and including plasma collisions. These results are then used to calculate the stochastic heating, which dominates at low pressures, and the ohmic heating, which dominates at high pressures. We determine the resulting plasma density, loaded resonator Q, and source coupling. The theory is compared to some preliminary experimental results.

I. INTRODUCTION

Plasma discharges are extensively used in the semiconductor industry for etching, sputtering and deposition processes, and their use has become critical for VLSI production. The current generation of parallel plate "diode", triode and downstream etchers is just adequate for present production devices and may not be suitable for submicron fabrication.

A variety of plasma sources are being investigated for advanced processing applications. We are studying a promising new plasma source, the helical resonator, which is well suited for advanced etching and CVD applications, because of its favorable ion bombardment characteristics and its ability to operate at pressures as low as 10^{-5} Torr. Helical resonator plasmas operate at ordinary radio frequencies (3-30 MHz), use simple inexpensive hardware, require no matching network and exhibit high Q (600-1500 typically without the plasma present) and a high characteristic impedance (Z_o). These resonators are a type of slow wave structure. As shown in Fig. 1, the source consists of a coil of prescribed diameter, pitch and length which is surrounded by a grounded coaxial cylinder. The composite structure becomes resonant when an integral number of quarter waves of the RF field just fit between the two ends. When this condition is satisfied, the intense electromagnetic fields within the helix can sustain a plasma with negligible matching loss down to very low background gas pressure.

In recent experiments[1-3], a rudimentary helical resonator etching apparatus was operable to as low a pressure as 10^{-5} Torr. At 0.1 mTorr pressure, a resonator discharge achieved a selectivity of more than 70:1 over silicon oxide and more than 1.7:1 over trilevel resist while anisotropically etching 0.25 μ undoped polysilicon gates across 100 mm wafers.[2-3] A resonator was also used for downstream deposition of high quality SiO_2 and p-SiN (plasma "silicon nitride") using an auxiliary RF supply to maintain controlled ion energy.[2-3] In another hot wall resonator configuration, dielectric films were deposited on wafers placed inside the plasma — with a furnace contained within the resonator and with no internal electrodes.[2-3] Helical resonators have been used for etching in the past — in this case chemical species from a high pressure (~1 Torr) discharge were used for downstream (isotropic) stripping.[4] However the special properties and versatility of helical resonator plasma sources have only come to light recently, when it was demonstrated that this structure can operate well at low pressure and generates ion

bombardment with characteristics that are especially effective for selective anisotropic etching of submicron features.

To understand the control parameter space, consisting of pressure, RF power, source length, plasma, helix, and outer cylinder radii, winding pitch angle, and excitation frequency, we must explore source operation both experimentally and theoretically and develop predictive models. A first step is to understand the helical slow wave modes in the source and their interaction with the plasma. We do this in three parts. First, we obtain the dispersion, β versus ω, and the relationship among the field quantities in the approximation of a cold, collisionless plasma and a "developed sheath helix" model, in which the r.f. current in the helix wires is replaced by a continuous current sheet ("sheath") and the cylindrical (r,θ,z) geometry is unfolded into a rectangular (x,y,z) geometry ("developed"). This is a standard analysis technique for treating helical systems[5] that retains most essential engineering physics. We use the results to explore the variation of propagation and resonance length with the variation of device parameters and plasma density. We then apply these results to a cylindrical system to calculate the electron heating due to bulk ohmic heating and surface stochastic heating and obtain a relationship between plasma density and power absorbed, for a given resonant device and neutral gas pressure. These results are used to calculate the coupling to the plasma and show that a matched condition is easily achieved. Finally, we compare the predictions, qualitatively, with some early experimental results.

II. COLD PLASMA, DEVELOPED SHEATH HELIX MODEL

A. Model Equations

The developed sheath model is shown in Fig. 2. The cylindrical (r,θ,z) system is "unfolded" to give the rectangular (x,y,z) system, with x and y playing the roles of r and θ, respectively. The system is uniform along y. The plasma thickness is a, the helix radius is b, and the outer conductor radius is c. The helix is modeled as an anisotropic sheet having infinite conductivity in the l direction and zero conductivity in the t direction, where the t and l directions make an angle ψ with respect to the y and z directions, respectively (see Fig. 2).

We assume wave solutions varying as $\exp j(\omega t - \beta z)$ for all field components. The axial fields satisfy the two dimensional Helmholtz equation

$$d^2E_z/dx^2 - \beta^2 E_z + k^2 E_z = 0 , \tag{1}$$

$$d^2H_z/dx^2 - \beta^2 H_z + k^2 H_z = 0 , \tag{2}$$

where $k = \omega/c_o$ is the free space wavenumber. We seek symmetric solutions in x for the longitudinal fields in the plasma, corresponding to the symmetric fields in r for the cylindrical system. We also require that the tangential E-field components vanish at the outer conductor surface. Integrating (1) and (2) and using these conditions, we obtain

$$E_{za} = A \cosh p_a x , \tag{3}$$

$$H_{za} = B \cosh p_a x , \tag{4}$$

$$E_{zb} = C \cosh p_o(x-a) + D \sinh p_o(x-a) , \tag{5}$$

$$H_{zb} = E \cosh p_o(x-a) + F \sinh p_o(x-a) , \tag{6}$$

$$E_{zc} = G \sinh p_o(x-c) , \tag{7}$$

$$H_{zc} = H \cosh p_o(x-c) . \tag{8}$$

Here the subscripts a, b, and c refer to the plasma, plasma-helix, and helix-wall regions, and where p_a and p_o are the transverse wavenumbers in the plasma and vacuum regions, respectively:

$$p_a^2 = \beta^2 - k^2\varepsilon_p , \tag{9}$$

$$p_o^2 = \beta^2 - k^2 , \tag{10}$$

where

$$\varepsilon_p = 1 - \frac{\omega_p^2}{\omega^2} \tag{11}$$

is the plasma permittivity, $\omega_p = (e^2 n/\varepsilon_o m)^{1/2}$ is the electron plasma frequency, e and m are the (positive) electron charge and mass, n is the electron density, and ε_o is the free space permittivity. For slow

waves, $\beta^2 > k^2$ and hence $p^2 > 0$ in both the plasma and the vacuum.

The transverse fields are obtained from the axial fields as:

$$E_x = \frac{j\beta}{p^2}\frac{dE_z}{dx}\,, \tag{12}$$

$$E_y = \frac{-j\omega\mu}{p^2}\frac{dH_z}{dx}\,, \tag{13}$$

$$H_x = \frac{j\beta}{p^2}\frac{dH_z}{dx}\,, \tag{14}$$

$$H_y = \frac{j\omega\varepsilon}{p^2}\frac{dE_z}{dx}\,, \tag{15}$$

where p and ε are the transverse wavenumber and permittivity appropriate to the particular region (a, b, or c) and μ is the free space permeability.

The boundary conditions at the plasma surface $x = a$ are that the tangential field components E_z, E_y, H_z and H_y are continuous. Using (3) - (6) along with (13) and (15), we obtain

$$C = A\cosh p_a a\,, \tag{16}$$

$$Fp_a = Bp_o \sinh p_a a\,, \tag{17}$$

$$E = B\cosh p_a a\,, \tag{18}$$

and

$$Dp_a\varepsilon_o = Ap_b\varepsilon_p \sinh p_a a\,. \tag{19}$$

At the helix surface $x = b$, the l and t components of the fields are given in terms of the y and z components as:

$$E_l = E_y\cos\psi + E_z\sin\psi\,, \tag{20}$$

$$E_t = -E_y\sin\psi + E_z\cos\psi\,, \tag{21}$$

$$H_l = H_y \cos\psi + H_z \sin\psi \,, \tag{22}$$

$$H_t = -H_y \sin\psi + H_z \cos\psi \,. \tag{23}$$

The boundary conditions at the helix surface are as follows: Because of the infinite conductivity of the surface in the l direction,

$$E_{lb} = E_{lc} = 0 \,. \tag{24}$$

Because of the zero conductivity in the t direction,

$$E_{tb} = E_{tc} \,. \tag{25}$$

There is no magnetic field discontinuity along the l direction because the surface current $K_t = 0$. Hence, we obtain

$$H_{lb} = H_{lc} \,. \tag{26}$$

Finally, the magnetic field discontinuity in the t direction yields a surface current component in the l direction:

$$K_l = H_{lb} - H_{lc} \,. \tag{27}$$

Inserting (20) - (23) into (24) - (26), we obtain the four equations:

$$-j\omega\mu\,[E \sinh p_o(b-a) + F \cosh p_o(b-a)] \cos\psi \tag{28}$$
$$+ p_o\,[C \cosh p_o(b-a) + D \sinh p_o(b-a)] \sin\psi = 0 \,,$$

$$j\omega\mu H \cos\psi = p_o G \sin\psi \,, \tag{29}$$

$$j\omega\mu\,[E \sinh p_o(b-a) + F \cosh p_o(b-a)] \sin\psi \tag{30}$$
$$+ p_o\,[C \cosh p_o(b-a) + D \sinh p_o(b-a)] \cos\psi =$$
$$j\omega\mu H \sinh p_o(b-c) \sin\psi + p_o G \sinh p_o(b-c) \cos\psi \,,$$

$$j\omega\varepsilon_o\,[C \sinh p_o(b-a) + D \cosh p_o(b-a)] \cos\psi \tag{31}$$
$$+ p_o\,[E \cosh p_o(b-a) + F \sinh p_o(b-a)] \sin\psi =$$

$$j\omega\varepsilon_o\, G \cosh p_o(b-c)\cos\psi + p_o\, H \cosh p_o(b-c)\sin\psi\ .$$

Equations (16) - (19) and (28) - (31) are eight linear, homogeneous equations for the eight coefficients A through H. For a non-zero solution set, the determinant of the coefficient matrix $[A]$ must vanish:

$$\det[A] = 0\ . \tag{32}$$

This yields the dispersion relation $\beta(\omega)$ for the modes. Knowing β for a given ω, we arbitrarily choose a mode amplitude such that $A = 1$. This normalizes $E_z = 1$ at $x = 0$. Next, we evaluate the coefficients B through H. From these, we obtain the amplitudes of all the electric and magnetic field components as a function of x. The surface current K_l is evaluated using (27).

B. Results and Discussion

The coefficient matrix was verified and (32) was solved to obtain the dispersion relation using the symbolic algebra computer system MACSYMA. A computer code HELIX was written to evaluate the dispersion relation, the coefficients, the fields, and the surface current. The standard source parameters were chosen to correspond approximately to an experimental device:

[ref]

$a = 3$ cm,

$b = 5$ cm,

$c = 10$ cm,

$L = 30$ cm,

$\psi = 0.1$ radians,

We consider the propagation at moderate plasma density, $n = 10^9$ cm^{-3}, at high density, $n = 10^{11}$ cm^{-3}, as well as without plasma.

Figure 3 gives β versus $f = \omega/2\pi$ with n as a parameter. For comparison, the upper and lower solid lines show a wave following the geometrical helix pitch,

$$\beta_h = \frac{2\pi f}{c_o \tan\psi}\ , \tag{33}$$

and a light wave $\beta_o = 2\pi f / c_o$, respectively. Without a plasma, there is only one mode of propagation,

with β somewhat smaller than β_h; ie, the wave velocity ω/β is somewhat *larger* than $c_o \tan\psi$. As n increases, the wave *speeds up*, and, as $n \to \infty$, $\omega/\beta \to c_o$. We call this the "coax" mode because, as we will see, for large n the plasma is at a high voltage with respect to the outer cylinder.

A second mode appears when n is such that $f_p^2 > f^2$, where

$$f_p = \omega_p/2\pi \approx 9000\sqrt{n} \ . \tag{34}$$

For $f_p = f = 20$ MHz, we find $n_p = n \approx 4.8\times10^6$ cm^{-3}. This is a low density compared to $n \geq 10^9$ cm^{-3} for typical discharge operation. Hence, both modes coexist during typical operation. The wave velocity for the second mode is always *smaller* than the helix velocity $c_o \tan\psi$. The mode appears as a resonance $\beta \to \infty$ at $n = n_p$, and the wave *slows down* as n increases. We call this the "helix" mode because, for large n, the plasma and outer cylinder are at nearly the same voltage, and the helix is at a high voltage with respect to them both.

At high densities, the axial wavenumbers for the two modes are very different. For example, at $n = 10^{11}$ cm^{-3}, β(coax) ≈ 0.5 m^{-1} and β(helix) ≈ 5.5 m^{-1}. Since the source length L is chosen to be roughly a quarter wavelength at the helix geometrical pitch, $\beta_h L \approx \pi/2$, the coax mode is not resonantly excited [β(coax) $\ll \beta_h$]. However, this mode does play a role in source operation at start-up; ie, when $n \approx 0$, the coax mode is near resonant excitation (see Fig. 3). However, during typical source operation ($n \geq 10^9$ cm^{-3}), only the helix mode is resonant, and it dominates the source operation. We concentrate on the coax mode for $n = 0$ and the helix mode for $n > 0$ in the results that follow.

As an example, for $L = 30$ cm and $\beta L = \pi/2$, we obtain $\beta \approx 5.2$ m^{-1}. Then from Fig. 3, we find the resonant frequencies for source operation: $f \approx 34$ MHz at $n = 0$, $f \approx 18$ MHz at $n = 10^9$ cm^{-3}, and $f \approx 21$ MHz at $n = 10^{11}$ cm^{-3}. The resonant frequency in the experiments, with the plasma present, was, in fact, found to be approximately at 20 MHz.

Figure 4 shows the magnitude of the field components versus x for the coax mode at start-up ($n = 0$) and the helix mode during source operation ($n = 10^9$ cm^{-3} and $n = 10^{11}$ cm^{-3}). Positive fields (+1 or $+j$) are indicated as solid lines through the computed values. We see that E_z is the dominant electric field component outside the plasma. Further, E_z is nearly independent of x within both the plasma-helix and helix-wall regions. This is true because $p_a a \ll 1$ and $p_o c \ll 1$; ie, the fields appear

to be quasistatic. For the helix mode, we also find that

$$\int_a^b E_x\,dx + \int_b^c E_x\,dx \approx 0\,. \tag{35}$$

Thus, the plasma surface at a and the conducting wall surface at c have roughly the same voltage. Inside the plasma, E_x is very small because $E_x(\text{plasma}) \sim E_x(\text{vacuum})\,\varepsilon_o/\varepsilon_p$ and $\varepsilon_o/\varepsilon_p \ll 1$.

E_z and E_y for the helix mode are peaked at the helix, and both fall to zero as $x \to c$. E_z within the plasma is roughly constant, while E_y is roughly linear with x. Within the plasma, $E_z > E_y$ at low density, but $E_y > E_z$ near the plasma edge at high density; both fields are larger than E_x. From the ordering of these field components, we conclude that E_x is critical for stochastic heating by the oscillating discharge sheath, while E_y and E_z play critical roles for ohmic discharge heating.

H_z is roughly constant in both the plasma-helix and helix-wall regions. We observe that the net axial magnetic flux is roughly zero:

$$\int_0^a H_z\,dx + \int_a^b H_z\,dx + \int_b^c H_z\,dx \approx 0\,. \tag{36}$$

H_y has the same general shape as E_x [compare (12) and (15)], except that H_y within the plasma does not change sign or suffer a reduction in magnitude due to the discontinuity in permittivity, as did E_x. Finally, H_x has exactly the same shape as E_y [compare (13) and (14)].

Figure 5 shows E_x just outside the helix (x = 5.1 cm) versus f, and Fig. 6 shows the surface current K_l versus f. The characteristic impedance Z_o can be determined from these data. If there are N turns in the coil, then

$$Z_o = N\,\frac{E_x\,(c-b)}{K_l L}\,. \tag{37}$$

For example, at $n = 10^{11}$ cm^{-3} and f = 20 MHz, we find $E_x \approx 2000$ and $K_l \approx 15$. For N = 48, we obtain $Z_o \approx 1100\ \Omega$.

Figure 7 shows the fields just outside the helix, the axial wavenumber β, and the surface current K_l as the plasma thickness a varies from 3 to 4.9 cm (helix position = 5 cm). We see a resonance in β as $a \to b$; thus, the presence of a gap between the plasma and the helix is essential to source operation.

Figure 8 shows the fields, β and K_l as the outer conducting wall position c varies from 5.5 to 10 cm. There is little effect on the dispersion characteristics. The wall is useful for RF shielding but plays little role in source operation over this range of variation in position.

Figure 9 shows the fields, β and K_l versus the plasma density n, with the frequency f as a parameter. The resonance and subsequent disappearance of the helix mode at $f_p = f$ is clearly seen in the dispersion characteristics.

III. CYLINDRICAL QUASISTATIC MODEL

A. Fields and Dispersion Relation

In the previous section, for the helix mode at typical discharge densities, we observed from the numerical results that:

(a) The transverse mode structure is quasistatic, $k \ll \beta$, and the transverse dimensions are such that $p_a a \ll 1$ and $p_o c \ll 1$.

(b) The net axial magnetic flux is approximately zero.

(c) The electric fields are small within the plasma, and the voltage between the plasma and the outer wall is approximately zero.

In addition, (12) - (15) correctly yield the transverse fields and (20) - (23) the l and t field components when r and θ are substituted for x and y respectively. Under these conditions, we can determine the fields, the dispersion relation, and the characteristic impedance for the helix mode in a cylindrical resonator containing a dissipative plasma (see Fig. 1) as follows:

From (a), $H_{za} = H_{zb}$ and H_{zc} are independent of r. Using (16), we obtain

$$H_{zb} - H_{zc} = K_\theta \,, \tag{39}$$

and from (b), we find that

$$\pi b^2 H_{zb} + \pi(c^2 - b^2) H_{cz} = 0 \,. \tag{40}$$

Solving (39) and (40), we obtain

$$H_{za} = H_{zb} = \frac{c^2-b^2}{c^2} K_\theta \,, \tag{41}$$

$$H_{zc} = -\frac{b^2}{c^2} K_\theta \,. \tag{42}$$

Applying Faraday's law to a circular path $r < b$,

$$2\pi r E_\theta = -j\omega\mu\pi r^2 H_z \,,$$

we obtain

$$E_{\theta a} = E_{\theta b} = -\frac{j\omega\mu}{2} \frac{c^2-b^2}{c^2} K_\theta r \,. \tag{43}$$

Similarly, we obtain

$$E_{\theta c} = -\frac{j\omega\mu}{2} \frac{b^2}{c^2} K_\theta \frac{c^2-r^2}{c^2 r} \,. \tag{44}$$

We note from (13) and (14) that

$$H_r = -\frac{\beta}{\omega\mu} E_\theta \,. \tag{45}$$

It follows also from (a) and (c) that E_r has an inverse r in the vacuum regions:

$$E_{rb} = \frac{-V}{r \ln(b/a)} \,, \tag{46}$$

$$E_{rc} = \frac{V}{r \ln(c/b)} \,, \tag{47}$$

where V is the helix voltage amplitude. Integrating (12) then yields

$$E_{zb} = -\frac{p_o^2}{j\beta} \frac{V \ln(r/a)}{\ln(b/a)} \,, \tag{48}$$

$$E_{zc} = -\frac{p_o^2}{j\beta} \frac{V \ln(c/r)}{\ln(c/b)} \,. \tag{49}$$

We note from (12) and (15) that

$$H_\theta = \frac{\omega\varepsilon}{\beta} E_r \,. \tag{50}$$

The normal component of the displacement vector is continuous across the plasma-vacuum interface:

$$\varepsilon_p E_{ra}(r=a) = \varepsilon_o E_{ra}(r=a) .$$

For subsequent use in calculating the power dissipated due to ohmic and stochastic heating, we include collisional effects in the plasma dielectric, modifying (11) to

$$\varepsilon_p = \varepsilon_o \left[1 - \frac{\omega_p^2}{\omega(\omega + j\nu)} \right], \tag{51}$$

where ν is the electron momentum transfer frequency. Using (51) and (46) and neglecting the displacement current in the plasma [the "1" in (51)], we obtain

$$E_{ra}(r=a) = \frac{\omega(\omega - j\nu)}{\omega_p^2} \frac{V}{a \ln(b/a)} .$$

Actually, $E_{ra} \sim I_1(p_a r)$, where I_1 is the modified Bessel function. Hence $E_{ra} \sim r$ to first order in $p_a r$. We then obtain

$$E_{ra} = \frac{\omega(\omega - j\nu)}{\omega_p^2} \frac{V}{a \ln(b/a)} \frac{r}{a} . \tag{52}$$

Similarly, $E_{za} \sim I_0(p_a r) \sim 1 + p_a^2 r^2/4$. Using this expansion along with (52) in (12) and integrating, we obtain

$$E_{za} = \frac{2\omega(\omega - j\nu)}{j\beta\omega_p^2 a} \frac{V}{a \ln(b/a)} . \tag{53}$$

Equations (41) - (50) and (52) - (53) give the quasistatic fields in terms of V and K_θ.

The dispersion relation $\beta(\omega)$ and the characteristic impedance Z_o follow from the boundary conditions (24) and (27). From (24), we obtain

$$E_{zb} = -E_{\theta b} \cot\psi$$

at $r = b$. Using this, together with (43) and (48), we obtain

$$V = \frac{\omega\mu\beta}{2p_o^2} \frac{c^2 - b^2}{c^2} K_\theta b \cot\psi . \tag{54}$$

From (27), we obtain

$$H_{\theta c} - H_{\theta b} = K_z = K_\theta \tan\psi \,. \tag{55}$$

Using (46) and (47) in (50) and inserting the result into (55), we obtain

$$K_\theta = V\frac{\omega\varepsilon_o}{\beta b}\left[\frac{1}{\ln(c/b)} + \frac{1}{\ln(b/a)}\right]\cot\psi \,. \tag{56}$$

Inserting (56) into (54) and using (10) for p_o^2, we obtain the dispersion relation

$$\beta^2 = g^2k^2\cot^2\psi + k^2 \,, \tag{57}$$

where

$$g^2 = \frac{c^2-b^2}{2c^2}\left[\frac{1}{\ln(c/b)} + \frac{1}{\ln(b/a)}\right] . \tag{58}$$

We note that this dispersion relation is equivalent to replacing the plasma by a perfect conductor for the TM part of the mode ($E_z \approx 0$), but allowing H_z to penetrate the plasma ($c_o/\omega_p \gg a$). For the usual ordering $\psi \ll 1$, the first term in (57) dominates. The quantity g is a correction factor for β of order unity with respect to a geometrical helix wave; ie, $\beta = g\beta_h$. As an example, for $a = 3$ cm, $b = 5$ cm, and $c = 10$ cm, we find $g \approx 1.13$. Comparing the result of (57), using the specific g from our example, to the exact dispersion characteristics for the developed helix in Fig. 3, we find that the result for β is close to, but somewhat smaller than, the result for the case $n = 10^{11}$ cm^{-3}, as expected.

For a helix having N turns in length L, we have $K_\theta L = NI$, where I is the helix current amplitude. Using this in (56), we obtain the characteristic impedance

$$Z_o = \zeta\sqrt{\frac{\mu_o}{\varepsilon_o}}\frac{Nb}{L} \,, \tag{59}$$

where

$$\zeta = \frac{g}{\dfrac{1}{\ln(c/b)} + \dfrac{1}{\ln(b/a)}} \tag{60}$$

is a geometrical factor. For a, b and c given previously, we find $\zeta \approx 0.33$. For our example, with $N = 48$ turns, we obtain $Z_o \approx 995\ \Omega$.

The axial structure of the fields is determined by the boundary conditions at the source ends. For a short circuit at $z = 0$ and an open circuit at $z = L$, we superimpose two positive and negative traveling waves of equal amplitudes to obtain

$$E_{ra} = -e_r \frac{\omega(\omega - j\nu)}{\omega_p^2} , \tag{61}$$

$$E_{\theta a} = e_\theta , \tag{62}$$

$$E_{za} = -e_z \frac{\omega(\omega - j\nu)}{\omega_p^2} , \tag{63}$$

where

$$e_r = -\frac{V_m}{a \ln(b/a)} \frac{r}{a} \sin \beta z , \tag{64}$$

$$e_\theta = -jV_m gk \frac{r}{b} \sin \beta z , \tag{65}$$

$$e_z = \frac{2j}{\beta a} \frac{V_m}{a \ln(b/a)} \cos \beta z , \tag{66}$$

and V_m is the helix voltage amplitude at the open circuit $z = L$. In writing (65), we have substituted (56) into (43) and used the first term in (57) for β^2.

The resonance condition is given by

$$\beta(\omega) L = \pi/2 . \tag{67}$$

Given L and using (57), we obtain the resonant frequency ω.

B. Ohmic and Stochastic Power

The r component of the RF current in the plasma is given by $J_r = j\omega\varepsilon_p E_{ra}$, or, using (51) and (61),

$$J_r = j\omega\varepsilon_o e_r . \tag{68}$$

The ohmic power per unit volume due to the E_r field is $p_r = \frac{1}{2}\mathrm{Re}(J_r^* E_r)$, or, using (61) and (68),

$$p_r = \tfrac{1}{2}\varepsilon_o \frac{\omega^2}{\omega_p^2} |e_r|^2 \nu \,. \tag{69}$$

Similarly, we obtain

$$J_\theta = \varepsilon_o \frac{\omega_p^2}{\nu + j\omega} e_\theta \,, \tag{70}$$

$$p_\theta = \tfrac{1}{2}\varepsilon_o \frac{\omega_p^2}{\omega^2+\nu^2} |e_\theta|^2 \nu \,, \tag{71}$$

$$J_z = j\omega\varepsilon_o e_z \,, \tag{72}$$

$$p_z = \tfrac{1}{2}\varepsilon_o \frac{\omega^2}{\omega_p^2} |e_z|^2 \nu \,. \tag{73}$$

Integrating (69), (71), and (73) over the plasma volume, we obtain the ohmic power dissipated in the plasma due to each field component:

$$P_r = \frac{1}{2}\varepsilon_o \nu \frac{\omega^2}{\omega_p^2} \left[\frac{V_m}{a \ln(b/a)}\right]^2 \frac{\pi a^2 L}{4} \,, \tag{74}$$

$$P_\theta = \frac{1}{2}\varepsilon_o \nu \frac{\omega^2}{\omega_p^2} \frac{\omega_p^4}{\omega^2(\omega^2+\nu^2)} \frac{a^2}{b^2} (kgV_m)^2 \frac{\pi a^2 L}{4} \,, \tag{75}$$

$$P_z = \frac{1}{2}\varepsilon_o \nu \frac{\omega^2}{\omega_p^2} \left[\frac{4L}{\pi a}\right]^2 \left[\frac{V_m}{a \ln(b/a)}\right]^2 \frac{\pi a^2 L}{2} \,. \tag{76}$$

We note that P_r and P_z are inversely proportional to n, while P_θ is directly proportional to n. For typical helical resonator parameters, P_θ is comparable to the other components only at the highest densities ($n \gtrsim 10^{11}$ cm^{-3}) and lowest pressures ($\nu \lesssim \omega$). We also note that

$$\frac{P_z}{P_r} = \frac{32}{\pi^2}\frac{L^2}{a^2} \gg 1 \,. \tag{77}$$

Therefore, the dominant electric field component for ohmic heating is E_z.

The stochastic heating power per unit length is given by[6-7]

$$S_{stoc} = K_{stoc}\left[\frac{s_0}{\lambda_D}\right]^{2/3}\frac{mu_e}{e^2 n_s}|J_{ro}|^2 2\pi a \ , \tag{78}$$

where

$$J_{ro} = -\frac{j\omega\varepsilon_o V_m}{a\ln(b/a)}\sin\beta z \tag{79}$$

is obtained from (68), s_0 is the self-consistent ion sheath thickness, $\lambda_D = (\varepsilon_o T_e/en_s)^{1/2}$ and n_s are the electron Debye length and the density, respectively, at the plasma-sheath edge, and $u_e = (8eT_e/\pi m)^{1/2}$ is the mean electron speed. The sheath thickness is found from the ion flux equation

$$en_s u_B = K_i\varepsilon_o\left[\frac{2e}{M}\right]^{1/2}\frac{\overline{V}^{3/2}}{s_0^2} \ , \tag{80}$$

where $u_B = (eT_e/M)^{1/2}$ is the Bohm (ion sound) velocity and $\overline{V}$ is the DC self-bias voltage across the sheath, given by

$$\overline{V} = K_{dc}V_{rf} \ , \tag{81}$$

where V_{rf} is the RF voltage amplitude across the sheath. V_{rf} is related to the maximum RF helix voltage amplitude by continuity of J_r:

$$\frac{K_{rf}V_{rf}}{s_0} = \frac{V_m}{a\ln(b/a)}\sin\beta z \ . \tag{82}$$

The dimensionless K factors for a self-consistent collisionless sheath are[6-7] $K_{stoc} \approx 0.34$, $K_i \approx 0.82$, $K_{rf} \approx 1.2$, and $K_{dc} \approx 0.83$.

Solving (80) - (82) for V_{rf} and s_0, with n_s taken to be constant in z, we obtain

$$V_{rf} = V_{rfm}\sin^4\beta z \ , \tag{83}$$

where

$$V_{rfm} = \frac{2K_i^2\varepsilon_o^2}{K_{dc}e^2 n_s^2 T_e}\left[\frac{K_{dc}V_m}{K_{rf}a\ln(b/a)}\right]^4 \tag{84}$$

is the maximum RF voltage amplitude across the sheath, and

$$\left[\frac{s_0}{\lambda_D}\right]^{2/3} = 2^{1/6}K_i^{1/3}\left[\frac{K_{dc}V_{rf}}{T_e}\right]^{1/2} . \tag{85}$$

Inserting (85) and (86) into (79) to eliminate s_0/λ_D and V_m^4/n_s^2, we find $S_{stoc} \propto V_{rfm}\cos^4\beta z$. Integrating this over z, we obtain the stochastic power

$$P_{stoc} = C_{stoc}\frac{\omega^2\varepsilon_o m}{e}u_e V_{rfm}\,2\pi aL , \tag{86}$$

where

$$C_{stoc} = \frac{3}{8}\frac{K_{stoc}K_{rf}^2}{2^{1/3}K_i^{2/3}K_{dc}} \approx 0.20 . \tag{87}$$

We also note from (82) and (83) that

$$s_0 = s_{0m}\sin^3\beta z , \tag{88}$$

where

$$s_{0m} = \frac{V_{rfm}}{V_m}K_{rf}\,a\ln\frac{b}{a} . \tag{89}$$

We compare the ohmic power $P_{ohm} = P_z$ to the stochastic power by letting $n = n_s(n/n_s)$ in (76) and using (84) in (76) to eliminate V_m^2/n_s:

$$P_{ohm} = C_{ohm}\frac{\omega^2\varepsilon_o m}{e}\nu a\,(V_{rfm}T_e)^{1/2}\frac{n_s}{n}\frac{L^2}{a^2}\,2\pi aL , \tag{90}$$

where

$$C_{ohm} = \frac{2^{1/2}}{\pi^2}\frac{K_{rf}^2}{K_{dc}^{3/2}K_i} \approx 0.33 . \tag{91}$$

From (86) and (91), we obtain

$$\frac{P_{ohm}}{P_{stoc}} = 1.65\frac{\nu a}{u_e}\frac{L^2}{a^2}\frac{n_s}{n}\left[\frac{T_e}{V_{rfm}}\right]^{1/2} . \tag{92}$$

We note the inequalities $(T_e/V_{rfm})^{1/2} \ll 1$ and $L^2/a^2 \gg 1$, which tend to cancel in (92). At low gas pressures, $\nu a/u_e \ll 1$, and stochastic heating dominates, while the converse holds at high pressures.

IV. POWER ABSORPTION AND COUPLING

The unloaded helical resonator is a naturally high-Q structure. If the resonator is matched through a coupling to an external power source the fields build up until the internal dissipation is equal to the supplied power. The coupling of energy to a plasma is relatively efficient both at low neutral pressure through the process of stochastic heating in the sheath, and at high pressure through ohmic heating in the bulk (glow) plasma. Because the resulting unloaded Q is relatively low, almost all of the power is deposited in the plasma when matched to the external source. Furthermore, the matching condition is easily achieved for the loaded Q.

For a given coupling that matches the Q with the plasma present, the resonator without the plasma is strongly overcoupled. Furthermore, as seen in Sec. II, the resonant frequency of the device shifts significantly with the plasma present. Thus, during startup, most of the power is reflected. Experimentally, this is not found to be a problem, as the normal operating power levels generate sufficient fields to create a plasma which builds up to the resonant, matched condition.

In this section, we treat separately both the low pressure case, in which stochastic heating dominates, and the higher pressure case where ohmic heating dominates. Actually, the two energy transfer mechanisms combine to determine the overall heating rate in a discharge. In its relation to the external driving field E_r, the stochastic sheath heating is similar to the heating in a capacitive RF discharge. The ohmic heating in the helical resonator is much stronger than in a capacitive discharge, because it is driven by a different and larger electric field component E_z, and therefore it becomes important at lower pressures.

The electron temperature and plasma density profile are determined by the balance between ion generation and loss to the plasma container wall. For low pressures, the electron temperature is uniform and the volume ionization rate in the bulk plasma is $\nu_{iz} n$, where $\nu_{iz} = K_{iz} p$ is the electron-neutral ionization frequency, K_{iz} is the rate constant and is a function of T_e alone, p is the neutral pressure, and n is the average bulk plasma density. Ions are lost radially to the wall, by free flow at the lowest pressures, $\lambda_i \geq a$, and by ambipolar diffusion at higher pressures, $\lambda_i \leq a$, where λ_i is the ion-neutral mean free path. For λ_i a constant, independent of ion energy, and for an ion thermal velocity

$u_{Ti} \ll u_{Di}$, the ion drift velocity, the diffusion coefficient is not a constant but is inversely proportional to u_{Di}. Godyak and Maximov[8] have determined the ion transport for a cylindrical plasma column under these assumptions, obtaining the approximate results

$$\nu_{iz} a \simeq \frac{2.2\, u_B}{(4 + a/\lambda_i)^{1/2}} \tag{93}$$

and

$$\frac{n_s}{n_0} \simeq \frac{0.8}{(4 + a/\lambda_i)^{1/2}} , \tag{94}$$

where n_0 is the on-axis plasma density. Equation (93) determines T_e given the pressure p. The density profile $n(r)$ is found to be relatively flat near the axis and to drop sharply near the plasma-sheath edge. Thus we take $n_0 \simeq n$, the average bulk density. Hence, (94) determines the ratio n_s/n.

Equation (93) is easily solved numerically for T_e, which we illustrate for argon in Fig. 10. However, here we take a simpler analytic approach in which we assume that the electron temperature is known, and use electron power balance to obtain the plasma density. This procedure gives reasonable results, because the exponential rate of ionization with electron temperature tends to freeze the temperature in a narrow range, within which the electron power balance is quite insensitive. For the case in which the stochastic sheath heating is dominant, the electron power balance depends only on the edge density, and therefore we do not require the solution (94) for the density ratio. In the ohmic heating case, both the average density and the edge density are required, so that (94) is required to obtain an complete solution.

A. Stochastic Heating

As in a capacitive RF discharge, the density at the plasma-sheath edge (beginning of the ion sheath) and the ion sheath thickness are found by solving the electron energy balance. The electron power leaving the discharge is

$$P_e = e n_s u_B \mathcal{E}_c\, 2\pi a L , \tag{95}$$

which when equated to the stochastic power (86) yields n_s. Using n_s in (84) and (89), we then can

evaluate s_{0m} and V_m, respectively. For example, assuming a reasonable value of $T_e \approx 4$ eV, we obtain

$$\begin{aligned} n_s &\approx 1.00\times 10^7 V_{rfm} \text{ cm}^{-3} \\ V_m &\approx 11.8\, V_{rfm}^{3/4} \text{ volts} \\ s_{0m} &\approx 0.156\, V_{rfm}^{1/4} \text{ cm} . \end{aligned} \tag{96}$$

Consider the device dimensions used in the analysis of the propagation and fields of our previous sections. Using the value of a typical V_{rfm} that might exist, $V_{rfm} = 700$ V, we obtain from (96) $n_s \approx 7.0\times 10^9$ cm^{-3}, $V_m \approx 1610$ V, and $s_{0m} \approx 0.80$ cm. The total power absorbed by the electrons is then obtained from (95) to be $P_e \approx 8.4$ W. The power P_i delivered to the ions is generated from the same flux, but multiplied by $\langle \overline{V} \rangle_z = K_{dc} \langle V_{rf} \rangle_z$, rather than $\mathcal{E}_c$. Averaging (83) over z yields $\langle \overline{V} \rangle_z = \frac{3}{8} K_{dc} V_{rfm}$. The total power absorbed by the plasma is then $P_{rf} = P_e + P_i \approx 51$ W.

From the field solutions we can obtain the energy stored in the helical resonator and therefore the resonator Q. The dominant field is the vacuum radial field, both between the helix and the plasma and between the helix and the outer conducting wall. The time-averaged stored energy is

$$W_T = 2\, W_E = \frac{1}{2}\varepsilon_o\, 2\pi \int_0^L dz \left[\int_a^b r dr\, |E_{rb}|^2 + \int_b^c r dr\, |E_{rc}|^2 \right] .$$

Using (46) and (47) with $V = V_m \sin \beta z$ gives

$$W_T = \pi \varepsilon_o V_m^2 \left[\frac{1}{\ln (b/a)} + \frac{1}{\ln (c/b)} \right] \frac{L}{2} . \tag{97}$$

Using the value of $V_m \approx 1610$ V for our example in (97), we obtain $W_T \approx 3.7\times 10^{-5}$ J. For a resonance frequency of $f_o \approx 20$ MHz and $P_{rf} \approx 51$ W, we then have the unloaded Q,

$$Q_U = \frac{2\pi f_o W_T}{P_{rf}} \approx 90 . \tag{98}$$

At match the loaded resonator Q, including the external loading, is half this value, $Q_L \approx 45$. The half power bandwidth is $f_o/Q_L \approx 0.44$ MHz. This value is consistent with the experimental observation that at a power level of 50 watts, a source frequency shift of 0.5 MHz produced a significant change in plasma parameters[1-3]. We note that the Q is sufficiently high to have a clear resonance, but the system

is not overly sensitive to small frequency shifts in the resonance.

The pressure regime for which stochastic heating dominates is found using (92). For $n_s/n \simeq 0.4$, which is the low pressure limit of (94), we find for our example with argon gas [$\lambda_i \simeq (300p)^{-1}$] that $\nu \simeq 4\times10^9 p$ and, hence, $P_{stoc} > P_{ohm}$ for $p \lesssim 2.3$ mTorr.

B. Ohmic Heating

Calculation of the energy deposited by ohmic heating is similar to that for stochastic heating, once the average density n is known. However, there is an additional complication in the energy balance in that the energy loss depends on the edge density n_s, thus requiring the use of (94) to relate n to n_s. In fact, this problem is also hidden in the previous solution in determining the resonant frequency. This latter effect is rather small, and we have neglected it.

For the electron energy balance, we equate (90) to (95), which yields an expression for n as a function of V_{rfm} and p:

$$n \simeq 2.9\times10^{11} p\, V_{rfm}^{1/2} \text{ cm}^{-3} .$$

Inserting $n \simeq n_0$ in (94) yields n_s. In the high pressure limit $a/\lambda_i \gg 1$ and for argon, we obtain

$$n_s \simeq 7.8\times10^9 p^{1/2} V_{rfm}^{1/2} \text{ cm}^{-3},$$

which is valid for $p \gg 4$ mTorr. Using this in (84) yields

$$V_m \simeq 330 p^{1/4} V_{rfm}^{1/2} \text{ volts},$$

and using (89), we obtain

$$s_{0m} \simeq 5.6\times10^{-3} p^{-1/4} V_{rfm}^{1/2} \text{ cm} .$$

For example, choosing $p = 0.1$ Torr and $V_{rfm} = 100$ V, we obtain $n \simeq 2.9\times10^{11}$ cm^{-3}, $n_s \simeq 2.5\times10^{10}$ cm^{-3}, $V_m \simeq 1860$ V, and $s_{0m} \simeq 0.10$ cm. The electron power from (95) is $P_e \simeq 30$ W, the ion power is $P_i = (\frac{3}{8} K_{dc} V_{rfm}/\mathcal{E}_c) P_e$ or $P_i \simeq 22$ W, and hence $P_{rf} \simeq 52$ W.

C. Coupling

Power can be very simply coupled from an external circuit to the resonator, and the condition for a match (critical coupling) can be obtained approximately from a perturbation analysis. Consider the RF generator and its transmission line to have characteristic impedances Z_S, with one side of the transmission line connected to the helix at the tap position z_T and the other side connected to the outer shield, as shown schematically in Fig. 1. Since the helix characteristic impedance Z_o given in (59) is typically large compared to Z_S, we expect a match to occur with the tap made near the shorted end of the helical resonator, where the voltage is small and the current is large.

From perturbation theory, the conductance seen at the position of the tap is

$$G_T = \frac{2P_{rf}}{|V_T|^2} , \tag{99}$$

where P_{rf} is the total RF power dissipated and

$$V_T = V_m \sin \beta z \tag{100}$$

is the helix voltage at the tap. For a match we require $G_T = Z_S^{-1}$. Substituting (100) in (99) and expanding for $\beta z_T \ll 1$, we obtain

$$V_m^2 \beta^2 z_T^2 = 2P_{rf} Z_S . \tag{101}$$

For our stochastic heating example with $\beta = \pi/(2L) \approx 0.052$ cm^{-1}, $P_{rf} \approx 51$ W, $V_m \approx 1610$ V and choosing $Z_S = 50\ \Omega$, we obtain $z_T \approx 0.85$ cm, corresponding to a tap between one and two turns, which was, in fact the approximate position found experimentally for efficient power transfer[1-3].

This research was supported by Department of Energy Grant DE-FG03-87ER13727 and by National Science Foundation Grant ECS-8517363.

REFERENCES

1. D.L. Flamm, D.E. Ibbotson, and W.L. Johnson, AT&T patent application (1989).

2. D.L. Flamm, as presented at the International Union for Pure and Applied Chemistry, 9th International Symposium on Plasma Chemistry, Sept. 7-15, Pungochiuso, Italy.

3. J.M. Cook, D.E. Ibbotson, and D.L. Flamm, 36th National Vacuum Symposium, Oct. 23-27,1989, Boston, MA; submitted to *J. Vac. Sci. Technol.* (1989).

4. G.N. Steinberg and A.R. Steinberg, U.S. Patent No. 4,368,092 issued Jan.11, 1983.

5. J.R. Pierce, *Traveling Wave Tubes*, D. Van Nostrand, New York, 1950, Cha. 3.

6. M.A. Lieberman, *IEEE Trans. Plasma Sci.* 17, 338 (1989).

7. G.R. Misium, A.J. Lichtenberg, and M.A. Lieberman, *J. Vac. Sci. Technol. A* 7, 1007 (1989).

8. V.A. Godyak and V.N. Maximov, *Vestnik Moskovskoy Universiteta*, ser. Fiz. Astr., 18, 51 (1977); see also V.A. Godyak, *Soviet Radio Frequency Discharge Research*, Delphic Associates, Falls Church, VA, 1986, p. 88.

FIGURE CAPTIONS

Fig. 1. Schematic of a helical resonator plasma source.

Fig. 2. Developed sheath model of helical resonator source.

Fig. 3. Axial wavenumber β versus frequency f for the coax and helix modes, with density n as a parameter. (O) helix mode, $n = 10^9$ cm^{-3}; (□) helix mode, $n = 10^{11}$ cm^{-3}; (+) coax mode, $n = 0$; (Δ) coax mode, $n = 10^9$ cm^{-3}; ($\times$) coax mode, $n = 10^{11}$ cm^{-3}.

Fig. 4. Magnitude of the field components versus position x. The solid lines denote a phase of +1 for E_y, E_z and H_x and a phase of $+j$ for E_x, H_y and H_z. (O) helix mode, $n = 10^9$ cm^{-3}; (□) helix mode, $n = 10^{11}$ cm^{-3}; (+) coax mode, $n = 0$.

Fig. 5. Magnitude of E_x just outside the helix ($x = 5.1$ cm) versus frequency f. The phase of E_x is $+j$. (O) helix mode, $n = 10^9$ cm^{-3}; (□) helix mode, $n = 10^{11}$ cm^{-3}; (+) coax mode, $n = 0$; (Δ) coax mode, $n = 10^9$ cm^{-3}; ($\times$) coax mode, $n = 10^{11}$ cm^{-3}.

Fig. 6. Magnitude of surface current K_l versus frequency f. The phase of K_l is $+j$. (O) helix mode, $n = 10^9$ cm^{-3}; (□) helix mode, $n = 10^{11}$ cm^{-3}; (+) coax mode, $n = 0$; (Δ) coax mode, $n = 10^9$ cm^{-3}; ($\times$) coax mode, $n = 10^{11}$ cm^{-3}.

Fig. 7. Magnitude of the fields just outside the helix ($x = 5.1$ cm), the axial wavenumber β, and the surface current K_l versus the plasma thickness a. (O) helix mode, $n = 10^9$ cm^{-3}; (□) helix mode, $n = 10^{11}$ cm^{-3}; (+) coax mode, $n = 0$.

Fig. 8. Magnitude of the fields just outside the helix ($x = 5.1$ cm), the axial wavenumber β, and the surface current K_l versus the outer conducting wall position c. (O) helix mode, $n = 10^9$ cm^{-3}; (□) helix mode, $n = 10^{11}$ cm^{-3}; (+) coax mode, $n = 0$.

Fig. 9. Magnitude of the fields just outside the helix ($x = 5.1$ cm), the axial wavenumber β, and the surface current K_l versus the density n, for the helix mode with the frequency f as a parameter. (O) $f = 5$ MHz; (□) $f = 10$ MHz; (+) $f = 20$ MHz; ($\times$) $f = 40$ MHz.

Fig. 10. Electron temperature T_e versus pressure p for an argon plasma with plasma radius $a = 3$ cm.

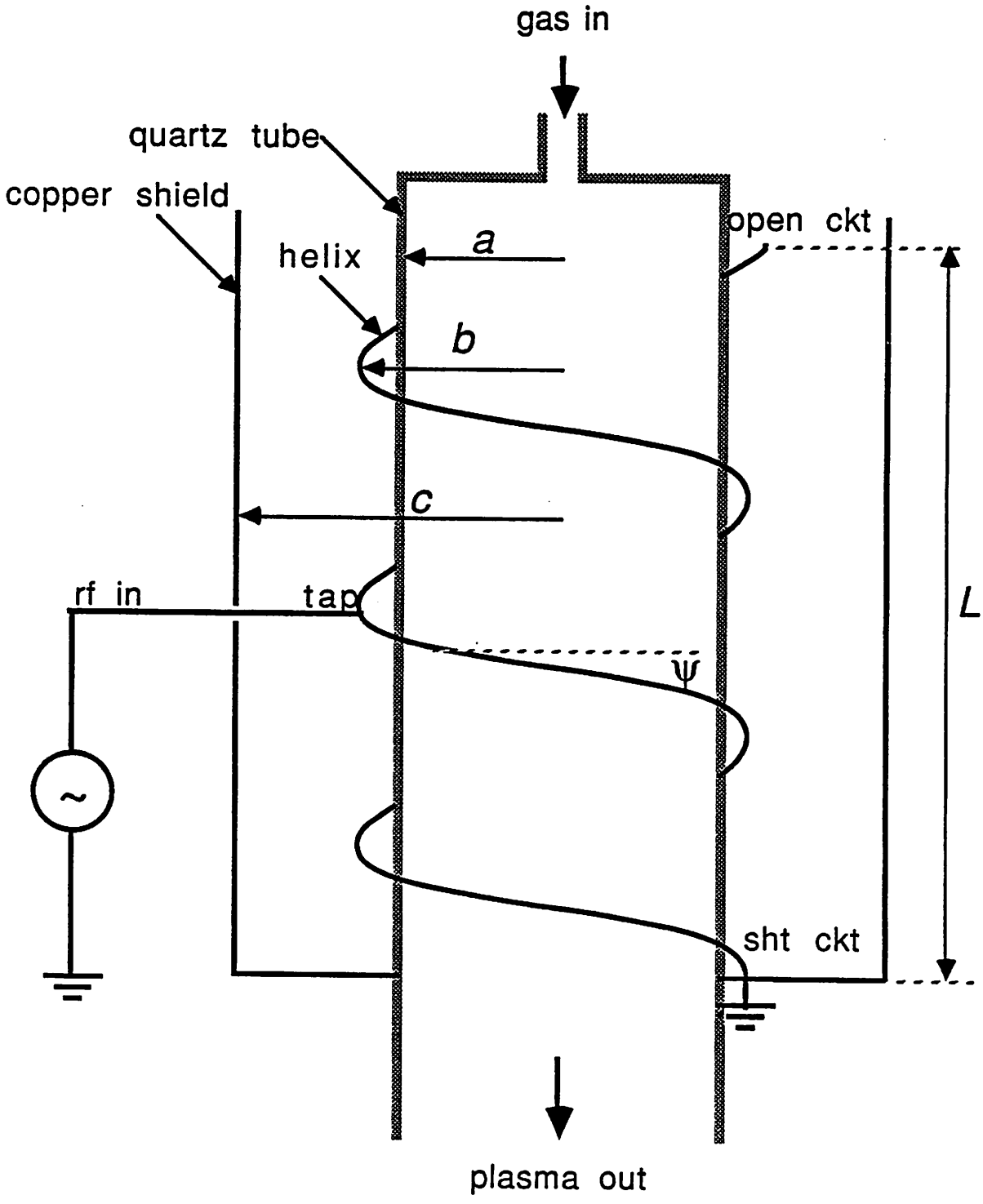
gas in
quartz tube
copper shield
helix
a
b
c
open ckt
rf in
tap
ψ
L
sht ckt
plasma out

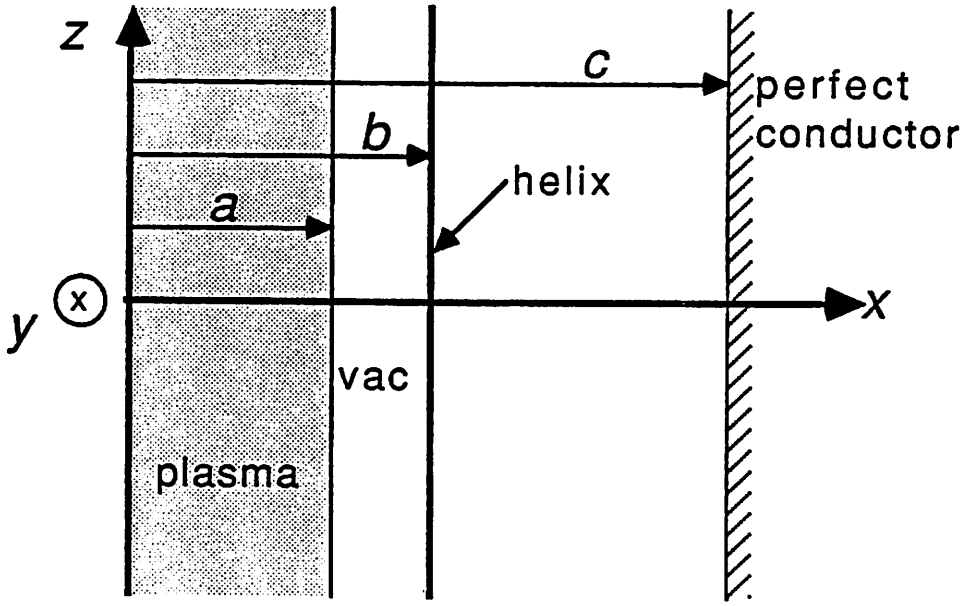
z
c
perfect
conductor
b
helix
a
y
x
x
vac
plasma

(a)

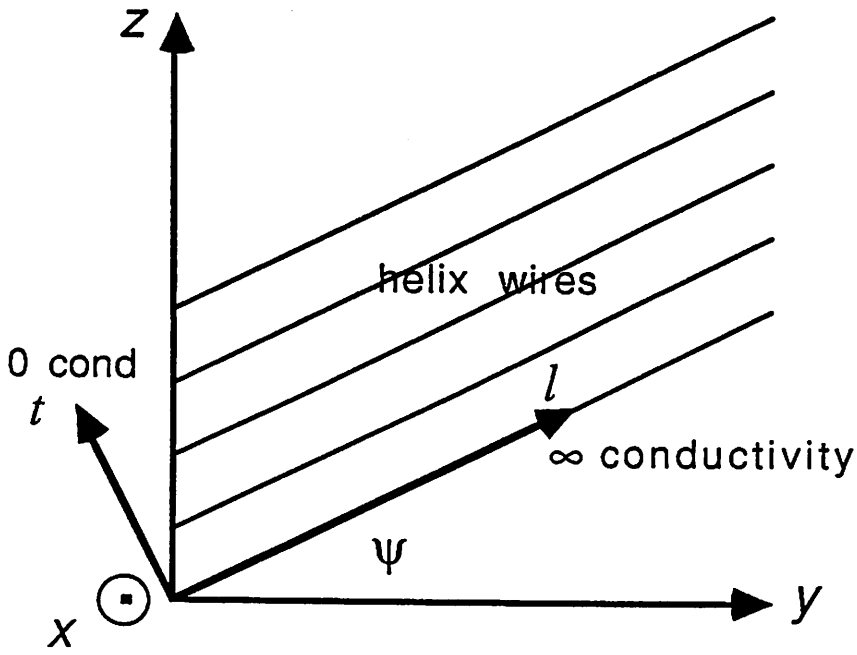
z
helix wires
0 cond
t
l
∞ conductivity
ψ
x
y

(b)

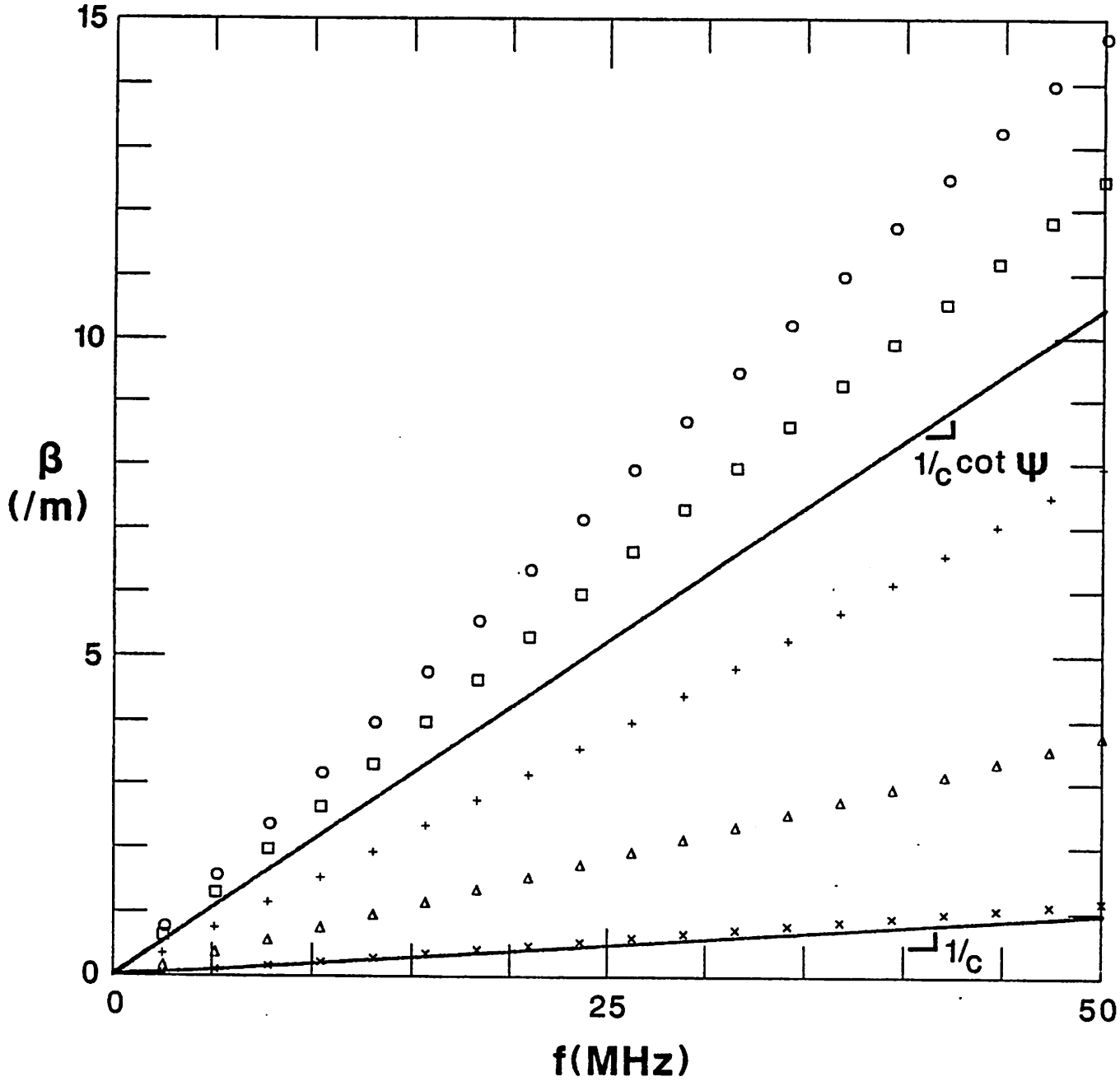
15
10
5
0
β
(/m)
0
25
50
f(MHz)
1/c cot ψ
1/c

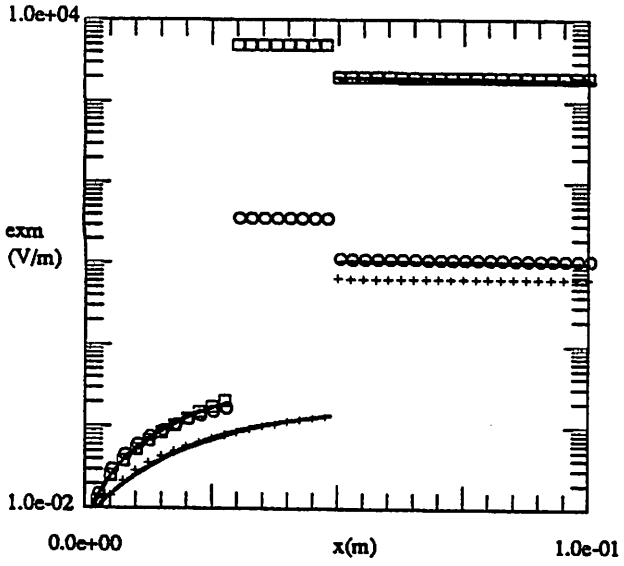
1.0e+04
exm
(V/m)
1.0e-02
0.0e+00
x(m)
1.0e-01

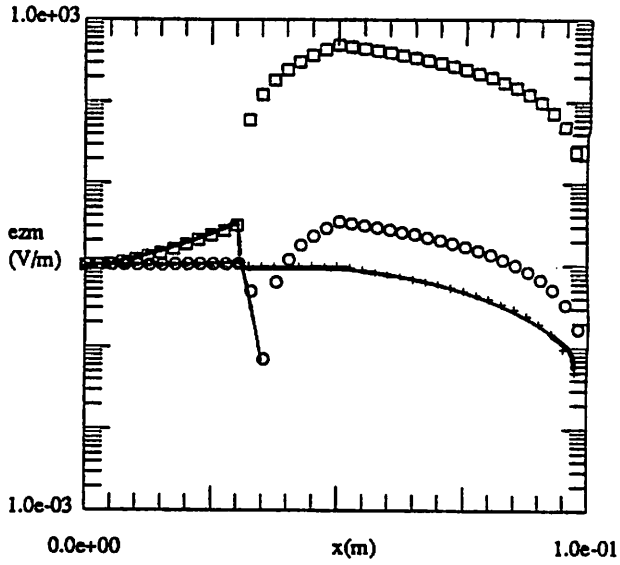
1.0e+03
ezm
(V/m)
1.0e-03
0.0e+00
x(m)
1.0e-01

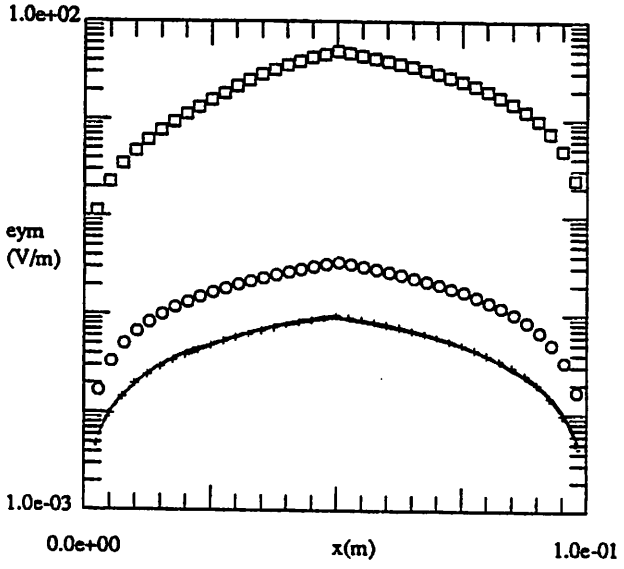
1.0e+02
eym
(V/m)
1.0e-03
0.0e+00
x(m)
1.0e-01

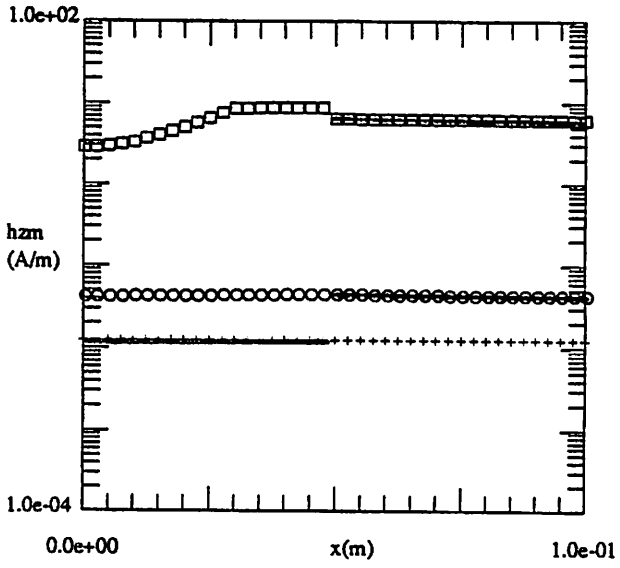
1.0e+02
hzm
(A/m)
1.0e-04
0.0e+00
x(m)
1.0e-01

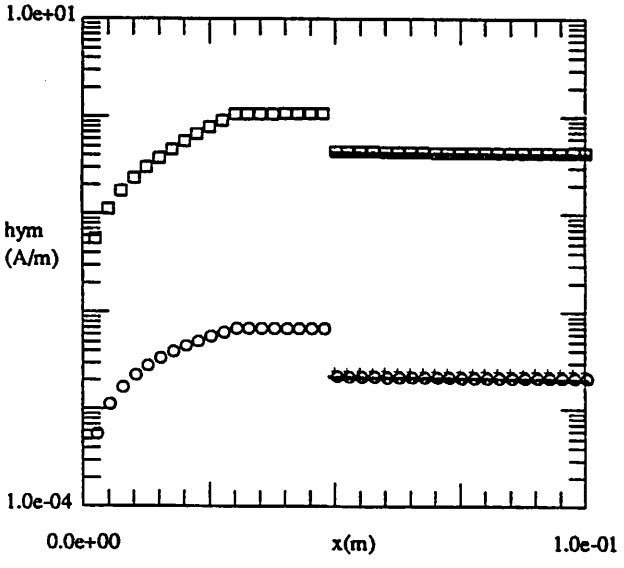
1.0e+01
hym
(A/m)
1.0e-04
0.0e+00
x(m)
1.0e-01

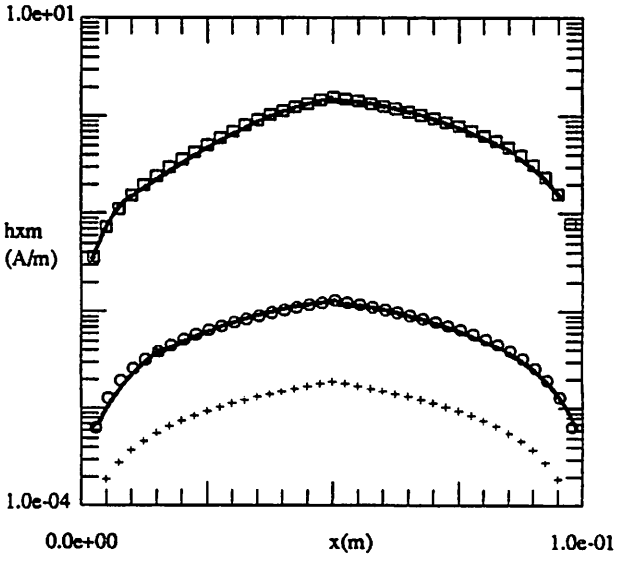
1.0e+01
hxm
(A/m)
1.0e-04
0.0e+00
x(m)
1.0e-01

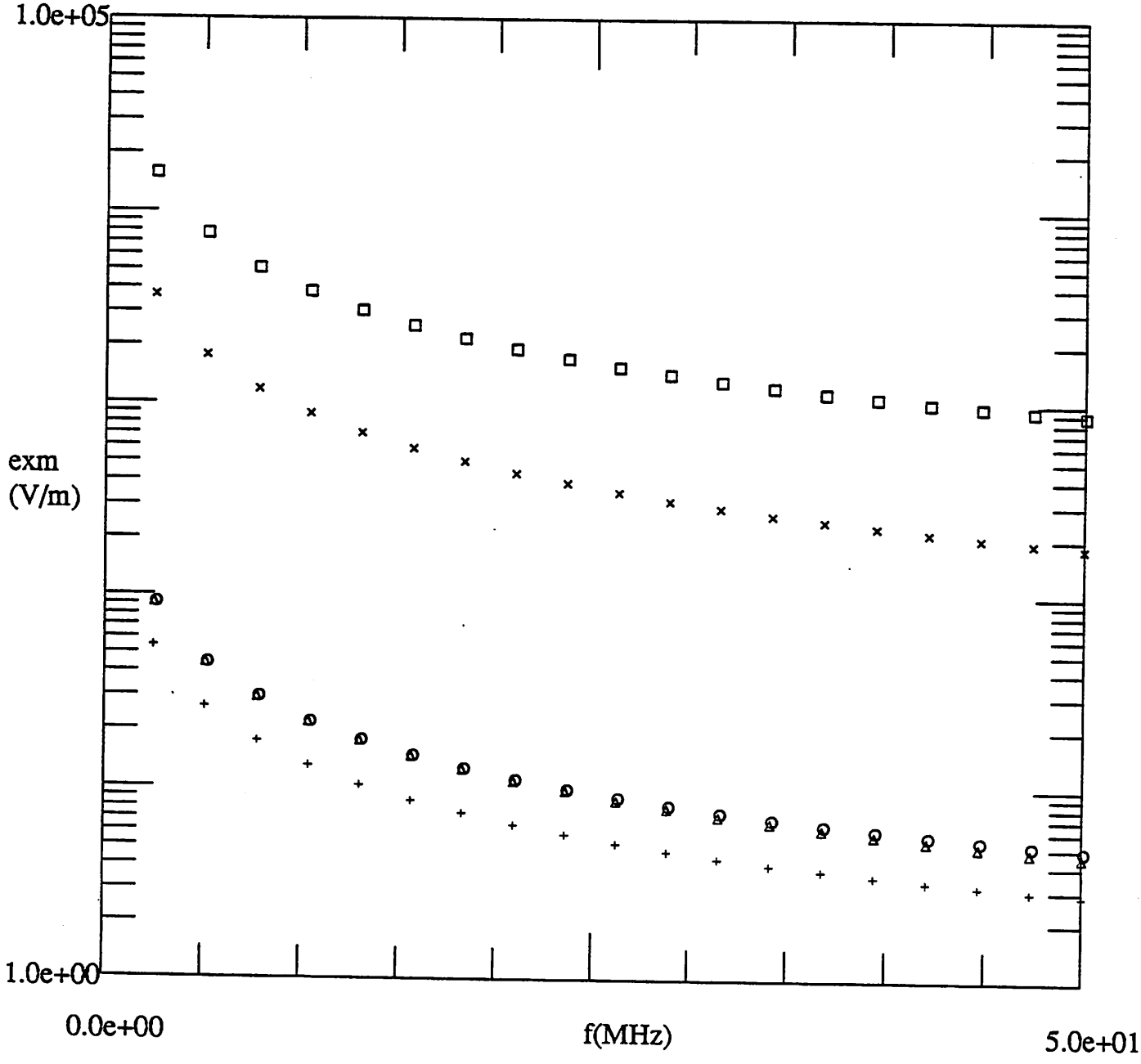
1.0e+05
exm
(V/m)
1.0e+00
0.0e+00
f(MHz)
5.0e+01

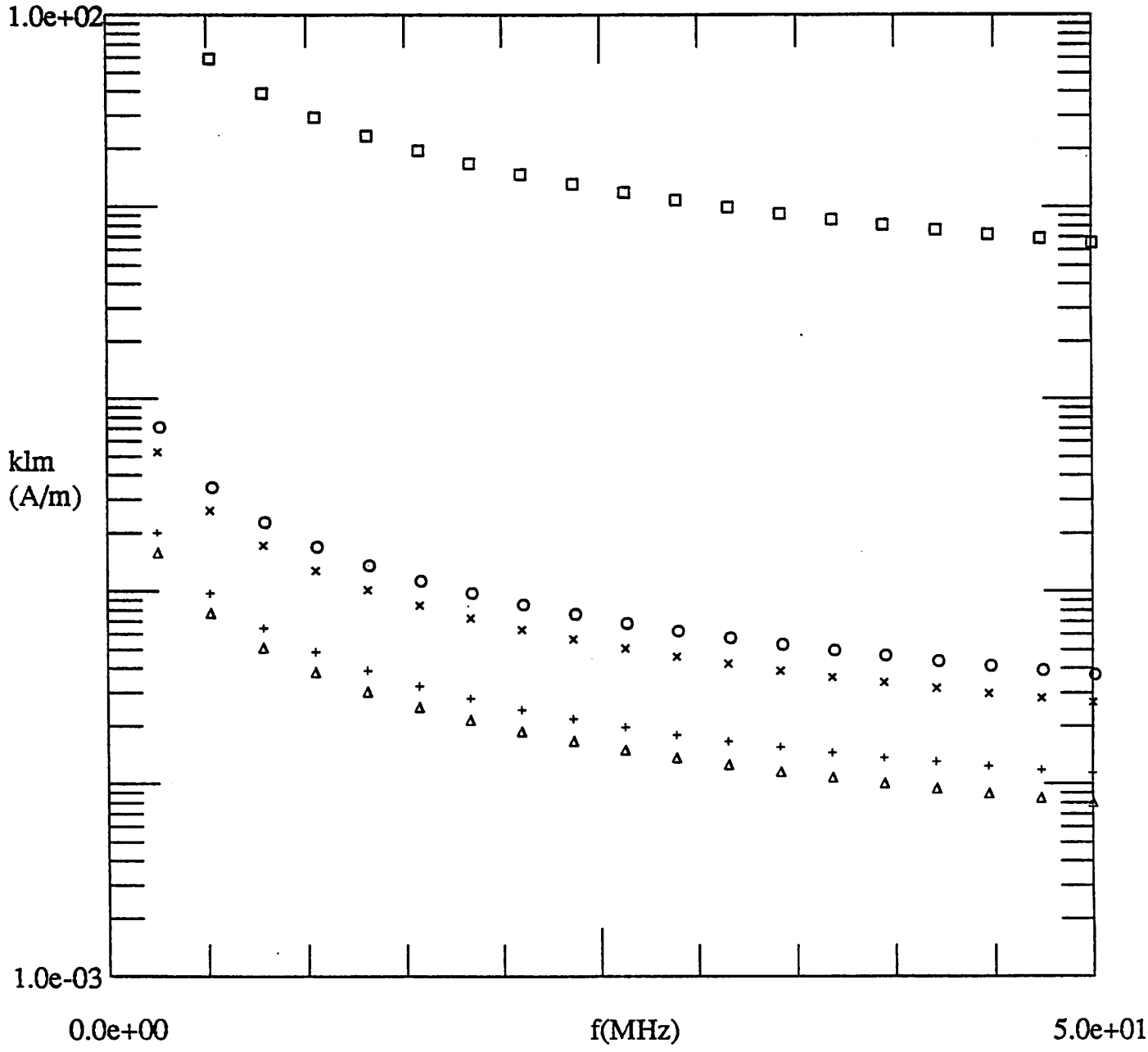
1.0e+02
klm
(A/m)
1.0e-03
0.0e+00
f(MHz)
5.0e+01

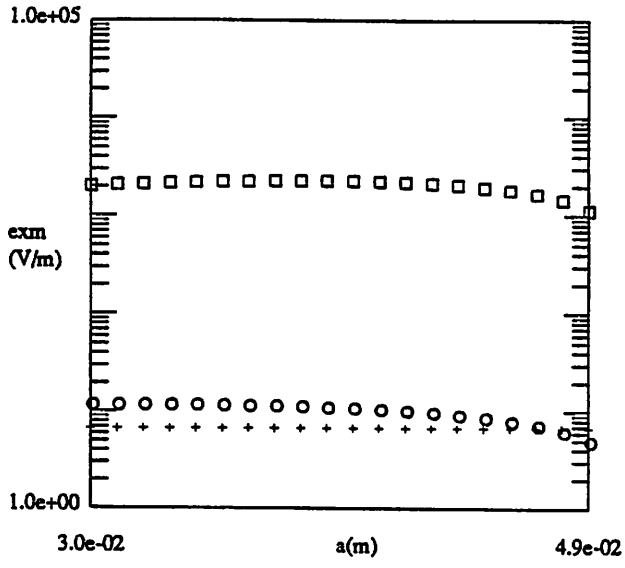
1.0e+05
exm
(V/m)
1.0e+00
3.0e-02
a(m)
4.9e-02

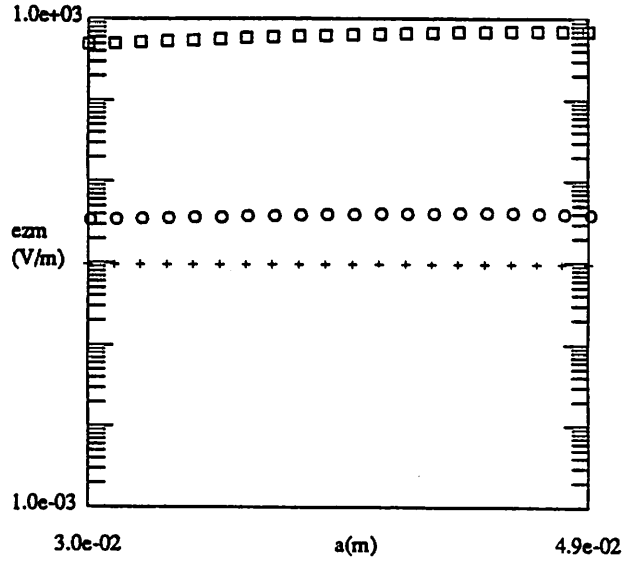
1.0e+03
ezm
(V/m)
1.0e-03
3.0e-02
a(m)
4.9e-02

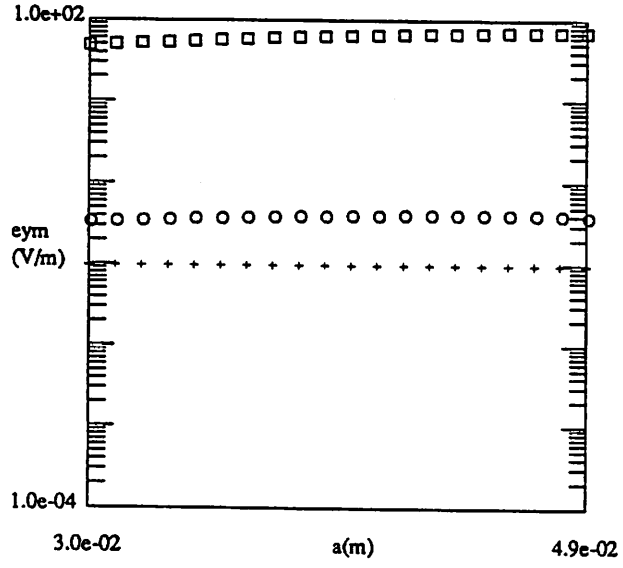
1.0e+02
eym
(V/m)
1.0e-04
3.0e-02
a(m)
4.9e-02

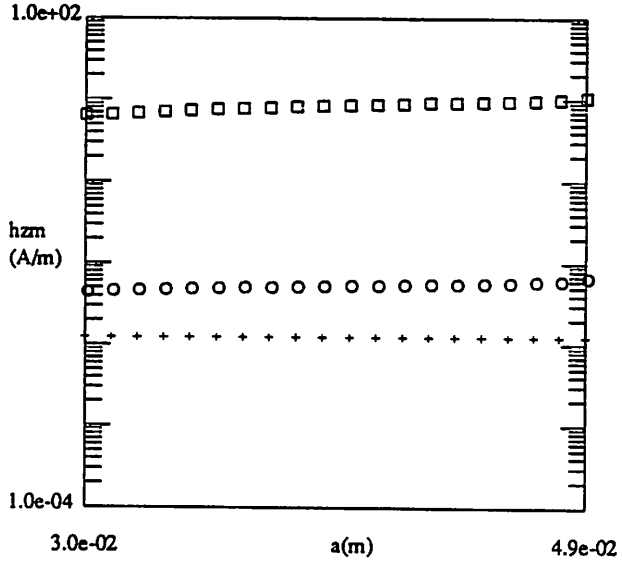
1.0e+02
hzm
(A/m)
1.0e-04
3.0e-02
a(m)
4.9e-02

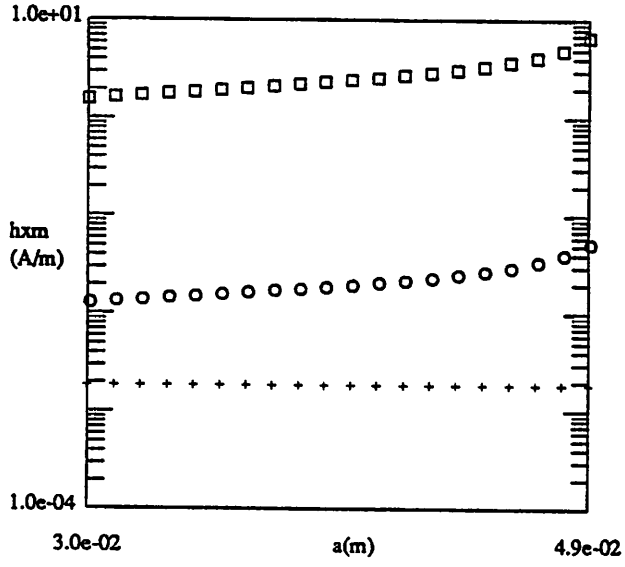
1.0e+01
hxm
(A/m)
1.0e-04
3.0e-02
a(m)
4.9e-02

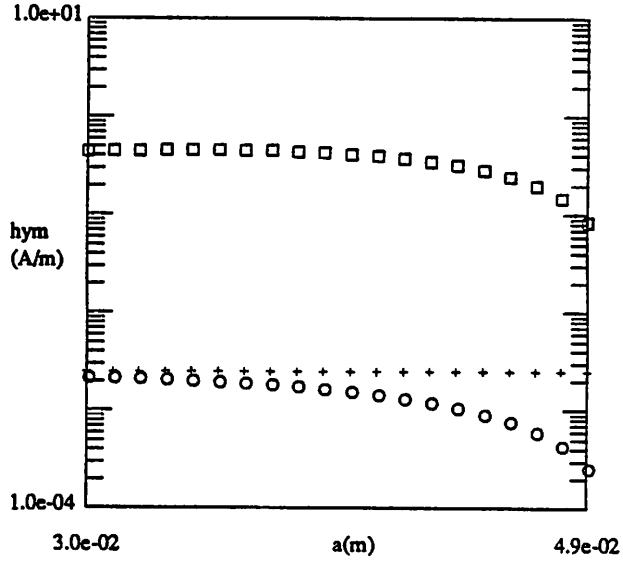
1.0e+01
hym
(A/m)
1.0e-04
3.0e-02
a(m)
4.9e-02

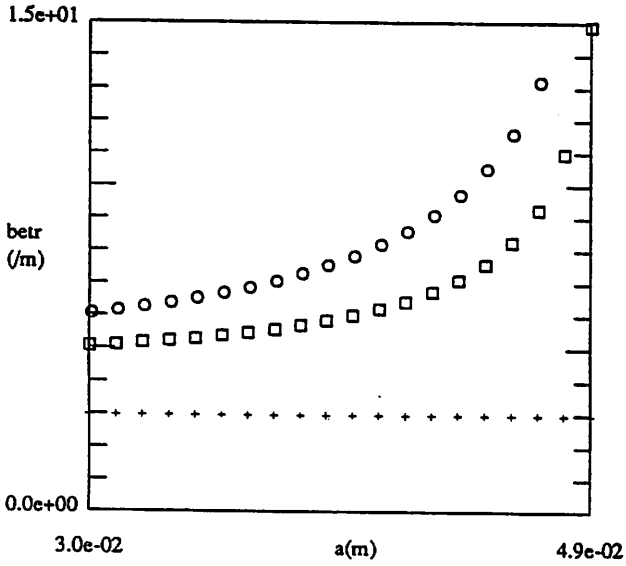
1.5e+01
betr
(/m)
0.0e+00
3.0e-02
a(m)
4.9e-02

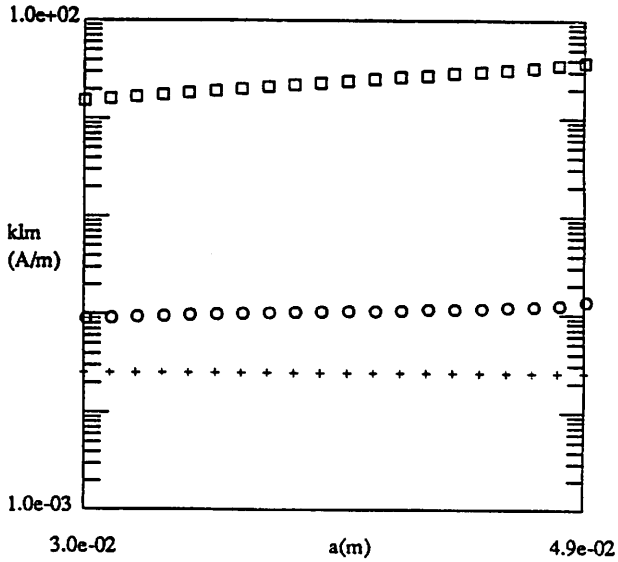
1.0e+02
klm
(A/m)
1.0e-03
3.0e-02
a(m)
4.9e-02

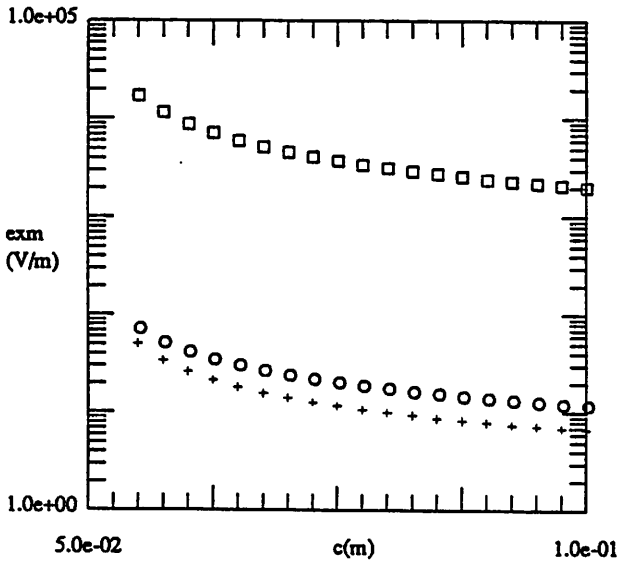
1.0e+05
exm
(V/m)
1.0e+00
5.0e-02
c(m)
1.0e-01

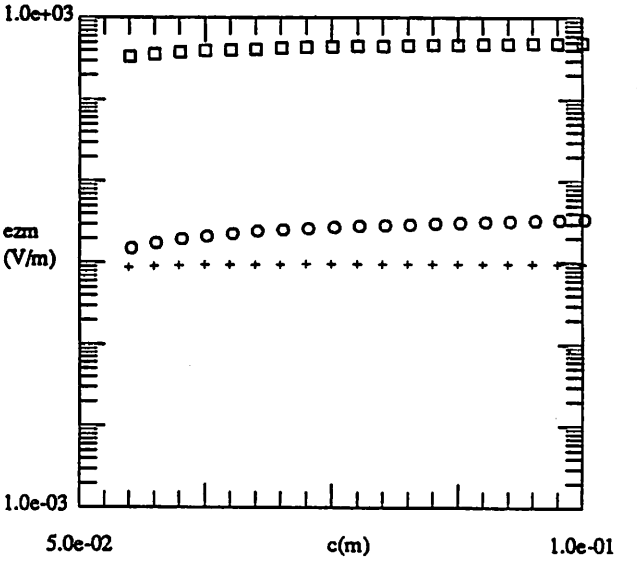
1.0e+03
ezm
(V/m)
1.0e-03
5.0e-02
c(m)
1.0e-01

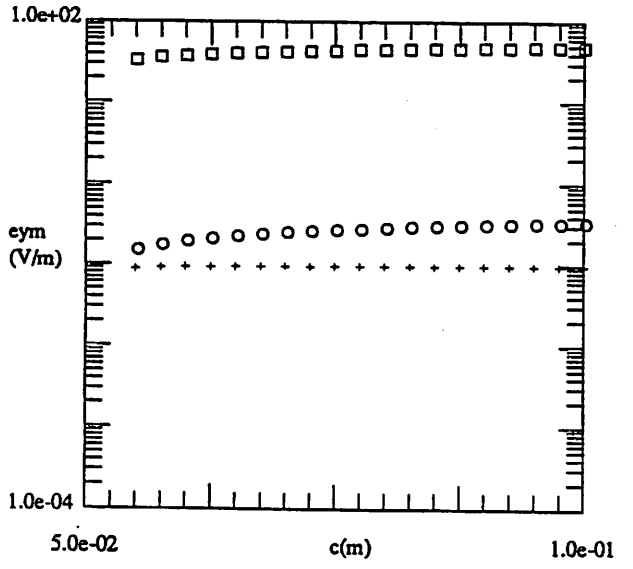
1.0e+02
eym
(V/m)
1.0e-04
5.0e-02
c(m)
1.0e-01

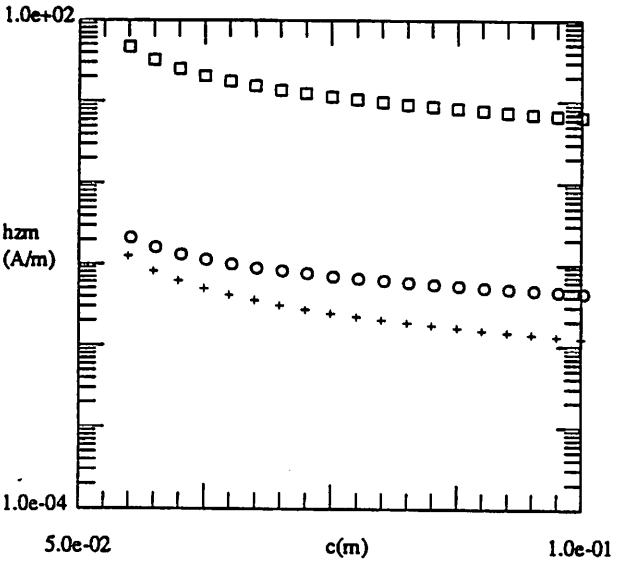
1.0e+02
hzm
(A/m)
1.0e-04
5.0e-02
c(m)
1.0e-01

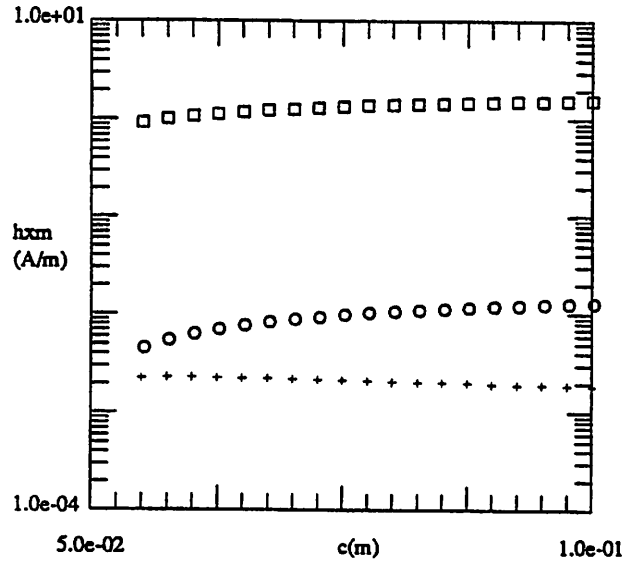
1.0e+01
hxm
(A/m)
1.0e-04
5.0e-02
c(m)
1.0e-01

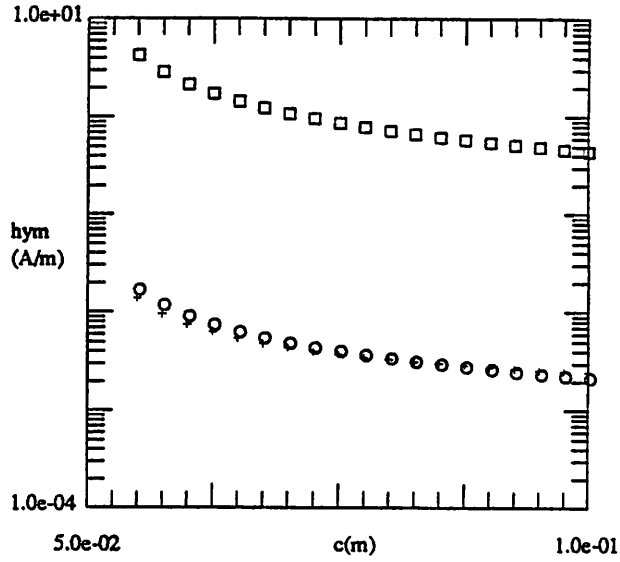
1.0e+01
hym
(A/m)
1.0e-04
5.0e-02
c(m)
1.0e-01

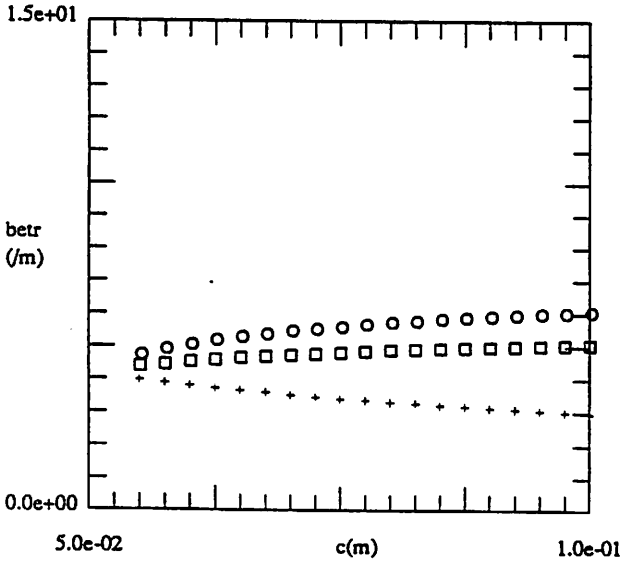
1.5e+01
betr
(/m)
0.0e+00
5.0e-02
c(m)
1.0e-01

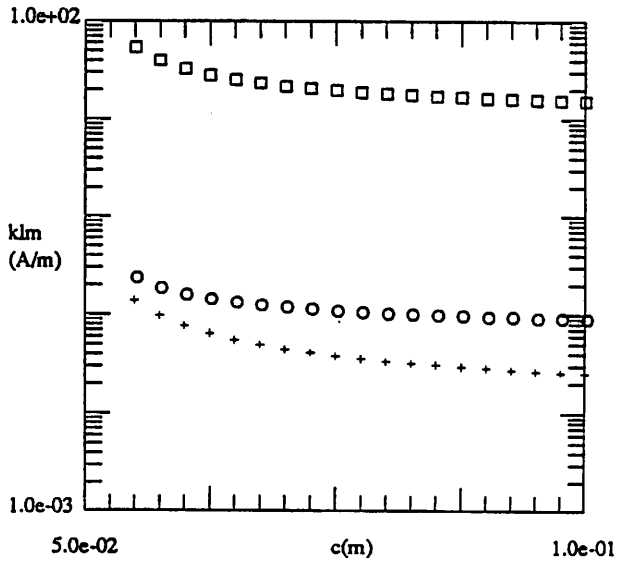
1.0e+02
klm
(A/m)
1.0e-03
5.0e-02
c(m)
1.0e-01

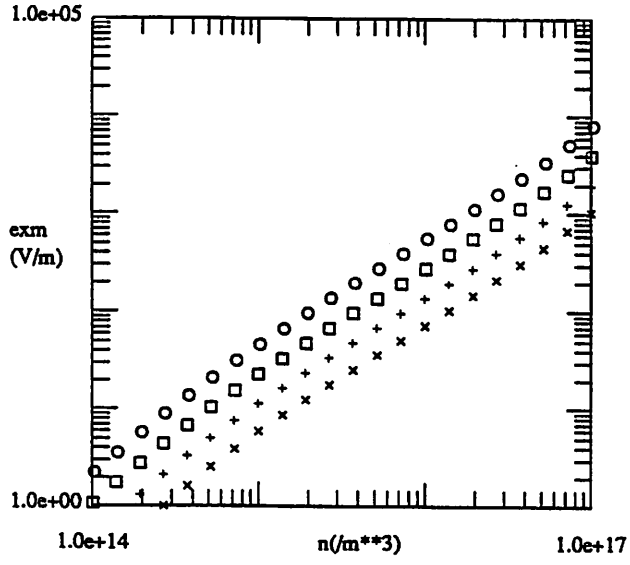
1.0e+05
exm
(V/m)
1.0e+00
1.0e+14
n(/m**3)
1.0e+17

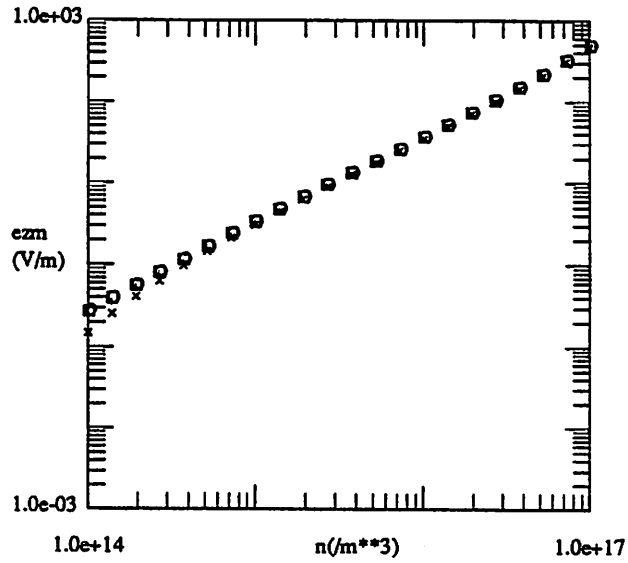
1.0e+03
ezm
(V/m)
1.0e-03
1.0e+14
n(/m**3)
1.0e+17

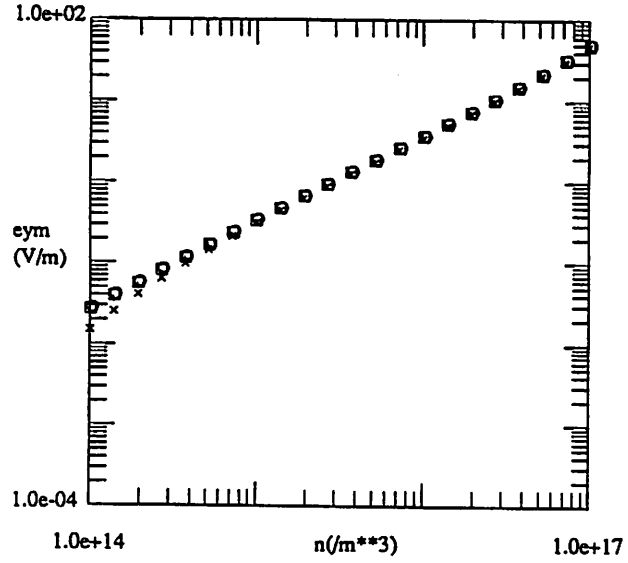
1.0e+02
eym
(V/m)
1.0e-04
1.0e+14
n(/m**3)
1.0e+17

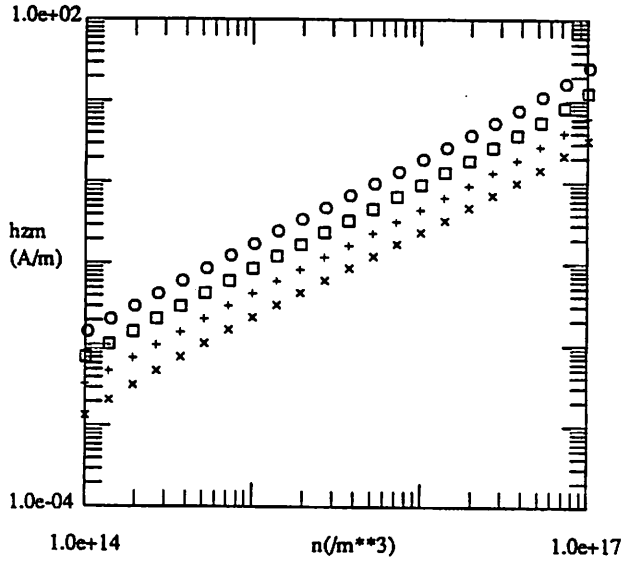
1.0e+02
hzm
(A/m)
1.0e-04
1.0e+14
n(/m**3)
1.0e+17

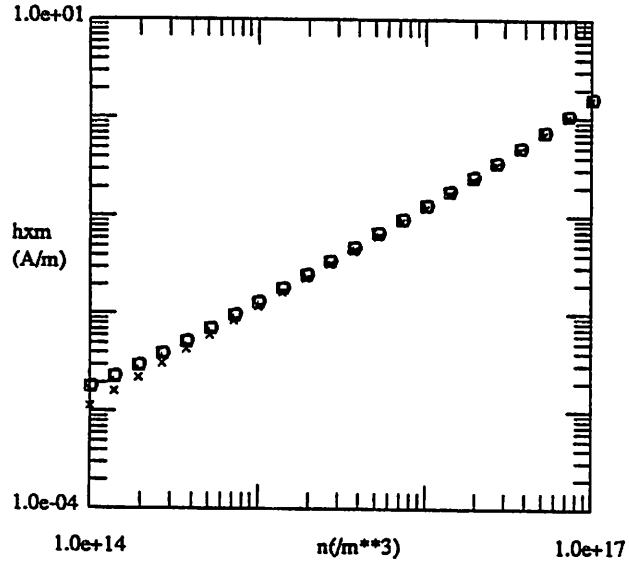
1.0e+01
hxm
(A/m)
1.0e-04
1.0e+14
n(/m**3)
1.0e+17

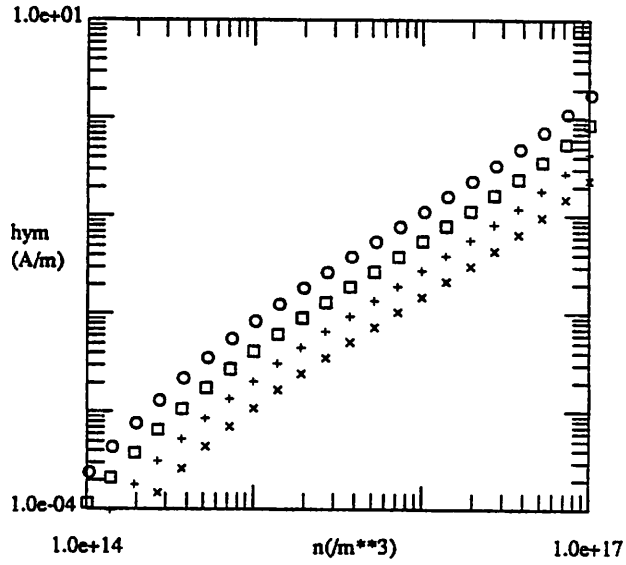
1.0e+01
hym
(A/m)
1.0e-04
1.0e+14
n(/m**3)
1.0e+17

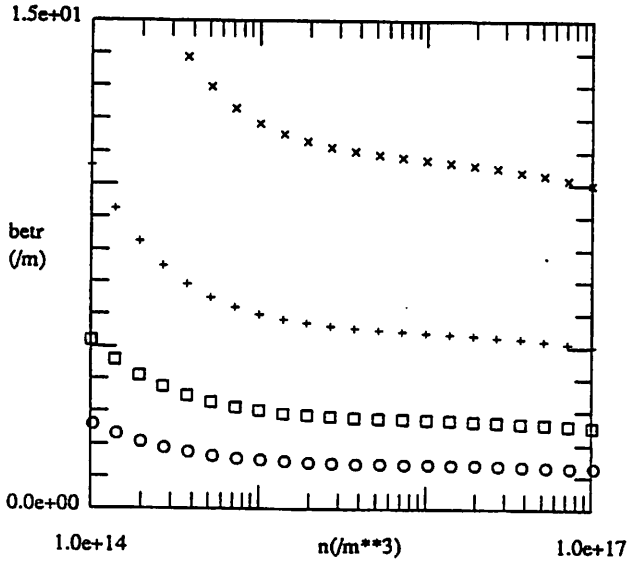
1.5e+01
betr
(/m)
0.0e+00
1.0e+14
n(/m**3)
1.0e+17

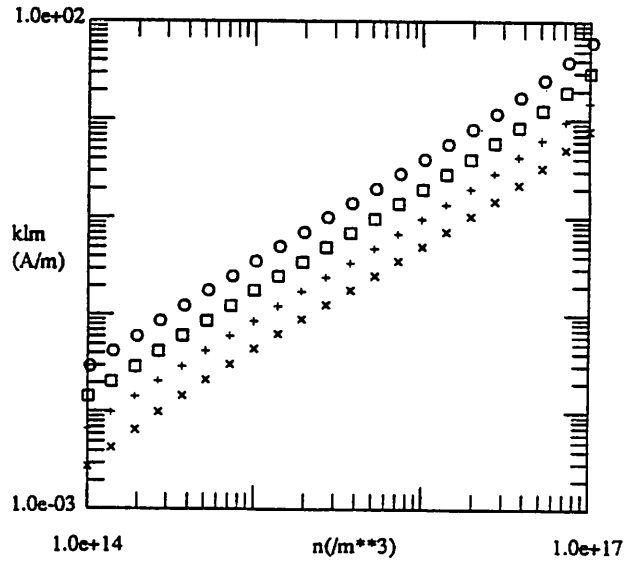
1.0e+02
klm
(A/m)
1.0e-03
1.0e+14
n(/m**3)
1.0e+17

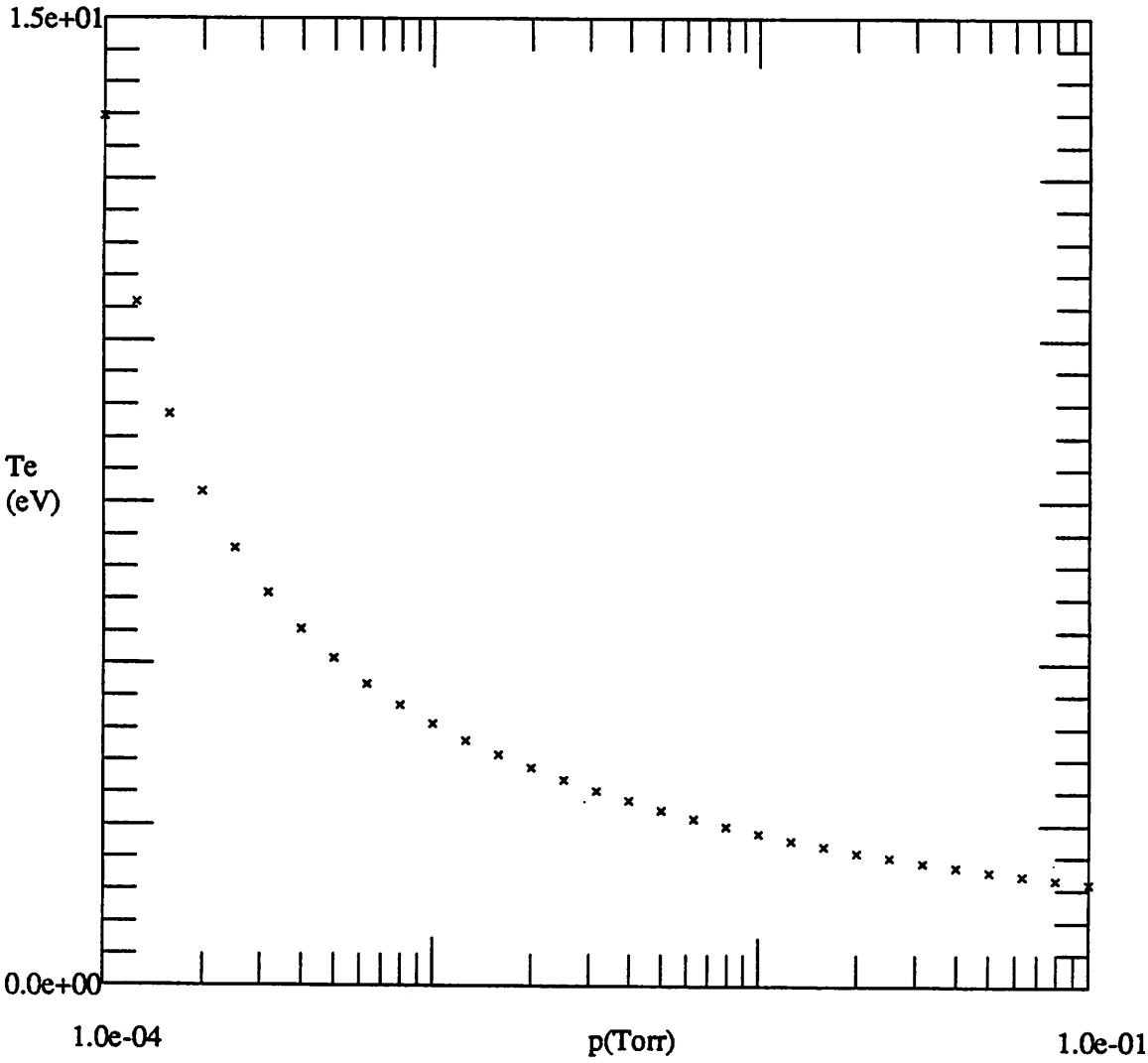

× CASE 1: a = 3 cm, argon gas